Human neck Finite Element model development and validation against original experimental data

Frank Meyer, Nicolas Bourdet, Caroline Deck, Remy Willinger, Jean-Sébastien Raul

Submission Number 04S-13

Stapp Car Crash Journal, Vol. 48 (November 2004), pp.

Human Neck Finite Element Model Development and Validation against Original Experimental Data

Meyer F., Bourdet N., Deck C., Willinger R.
Strasbourg University, ULP-IMFS-CNRS7507, 2 rue Boussingault 67000 Strasbourg, France

Raul J.S.
Institute for forensic Science, ULP, 11 rue Humann 67085 Strasbourg, France

ABSTRACT – This study proposes a detailed FEM of a human volunteer's neck and proceeds to an original model validation against experimental data recorded with this human volunteer. In order to evaluate the new model against existing data a successful temporal validation of the model was obtained under frontal, lateral, oblique and rear impact. New validation parameters are based on an experimental test proceeded in the frequency domain in order to extract the volunteer's Head-Neck system's modal characteristics. In deep validation of the head neck FEM is then performed by superposing the numerical and experimental frequency response function. Model optimisation in the frequency domain permitted after significant properties modification to reproduced accurately both, the neck extension mode at 1.4 Hz and the head retraction mode at 8.8 Hz. Finally the "frequency domain optimised" FEM response was superimposed with the temporal corridors provided in the literature. It must be mentioned that the model's response in the temporal domain remains inside existing corridors after this model optimisation in the frequency domain illustrating that the temporal validation is not accurate enough. This study proposes a neck model with improved geometry description and biofidelity with special attention paid to the retraction mode, a phenomenon which is often masked in the temporal domain.

KEYWORDS – Modal analysis, Finite element neck model, Validation.

INTRODUCTION

In spite of a large number of research projects in the field of cervical spine biomechanics, current protection systems are still not capable of significantly reducing low-AIS lesions, lesions that generate considerable costs to society (Deng et al., 2000). The main reason for this failure is the inability of the medical profession to diagnose the origin of the pains that victims of these accidents complain of. This is why scientists, who have over many years undertaken experimental and theoretical studies to try to better understand the mechanical behaviour of the head-neck system during an impact, have encountered so many difficulties in their approach. First of all, series of tests designed to describe the response of the cervical column under impact have been undertaken. As far as these experiments characterising the behaviour of this complex segment under impact are concerned, we will not list here all the characterisations that have been carried out. On the other hand, a review of the data most commonly used to validate the Finite Element Models (FEM) of the cervical column will be done.

The tests carried out by the N.B.D.L (National Biodynamics Laboratory) reported by Ewing et al. (1968, 1977) with frontal, lateral and oblique impacts are frequently used as a basis for the validation for finite element models of the neck : Dauvilliers (1994), De Jager et al. (1996), Nitsche et al. (1996), Happee et al. (1998), Yang et al. (1998) and Astori et al. (1998)). The advantages of such a validation include two important aspects : the first lies in the fact that the tests were carried out on volunteers subjected to high intensity impacts, thus leading to the non-linearity of the neck. Secondarily, these tests were very well instrumented, thus allowing the recording of the accelerations at the first thoracic vertebra T1, which constitutes the initial conditions in the modelling. As for the recording of the six head accelerations components, three linear and three rotational accelerations were fixed at head level and this constitutes the basis for the validation of the FEMs. However, it is clear that in spite of the

complete instrumentation of the test subject, the FEM reproduce correctly only the kinematics of the head.

Over the last few years we have seen the emergence of new experiments determining the movements relating to the cervical vertebrae during a rear impact (movements of the articular surfaces as well as the bodies of the vertebrae). In this line of research, two studies are essential, that of Ono et al. (1997) on 12 volunteers and that of Deng et al. (2000) on 6 cadavers. These studies are a significant step in the attempt to correctly reproduce the behaviour of the spine from a local point of view. These experiments allow us not to limit ourselves to only the movements of the anatomical centre of the head, unlike the classic tests.

However, at the present time, none of these investigations have succeeded in determining firmly the reasons why patients complain of neck pain, nausea or muscular pain after a low intensity rear impact (Ovadia et al. 2002). Alongside the experiments considering the whole of the head-neck system, local approaches have attempted to characterise behavioural laws concerning the intervertebral discs, ligaments and muscles.

Furthermore, in spite of all these highly instrumented experiments that give access to the kinematics of the head, or to the relative movements of the vertebrae, these validation data are always expressed in the form of an experimental corridor where the minimum and the maximum recorded values define the range of validity of an FEM. Most often these corridors are wide, and the response of the model may present inclines with very variable origins, oscillations or acceleration peaks whilst remaining within the area considered, but implying very varied characteristics of the model. These factors are in fact of considerable importance for the identification of the mechanical systems, but cannot be taken into account in this temporal approach, which is always difficult in impact situations.

The aim of this study is first to construct an FEM of the upper spine with a high degree of geometrical accuracy, to evaluate it in comparison to the tests generally accepted by the scientific community considering the kinematics of the head in front, lateral and oblique impact situations (N.B.D.L.) and a rear impact situation (Prasad et al., 1997).

Impulse experiments carried out in the sagittal plane will then allow the modal characteristics of the head-neck system to be extracted. A numerical frequency analysis will be carried out on the neck FEM with a view to comparing the natural frequencies of the model and of the volunteer. The optimisation of the model will allow us to numerically reproduce the experimental modal behaviour. The temporal validation of the optimised model in the frequency domain will show that the adjustment of the mechanical properties on the temporal response alone is not enough to ensure biofaithful behaviour.

METHODS

Model geometry

It is possible to distinguish in the bibliography two families of FEM of the cervical column. The models that represent an average cervical spine (De Jager et al. (1996), Nitsche et al. (1996), Dauvillier (1994), Astori (1998)) and those obtained by generating a mesh from scanner or IRM sections of volunteers, a method used by Camacho et al. in 1997 and Yang et al. in 1998.

For our study and because we are focusing on a specific volunteer, it seemed to us essential to base our work on the geometry of a living human subject of average size and close to 50th percentile male : [Height: 1.72 m, weight: 72 Kg, age: 33 years]. This approach allows us not to make any approximation regarding the geometry of the cervical vertebrae. From a modelling point of view, we have taken millimetric scanner[1] sections of the subject. These scanner sections then underwent grey level processing in order to extract the bone part of the cervical column and of the skull. A rough tria mesh in STL format was then constructed as shown in figure 1.

This file was then imported under the Hypermesh V6.0 meshing software so that the cervical vertebrae could be completely meshed. Indeed, the explicit finite element calculation codes used in the crash field, such as Radioss, require regular meshing that checks certain geometrical criteria influencing the calculation time pitch. Table 1 recapitulates the

[1] The files of the CT scan used were obtained from a ct scan performed on a medical member of our team. The scan was initially performed for diagnosis purpose. The results of the ct scan being normal, the idea appeared to use the files obtained. The files were then anonymized and transmitted to our institution. We insist on the fact that the ct scan was performed for medical purpose and not for our study. We simply jumped on this opportunity. Furthermore it was performed on a doctor who had a perfect knowledge of the consequences of this imaging technique and the possible benefit of the ct scan was greater than the risks of ignoring a severe injury of the cervical spine.

values of these criteria used throughout the meshing process.

TABLE 1. Meshing criteria allowing the calculation time to be optimised.

Criterion	***Values***
Length min.	2.25 mm
Length max.	3 mm
aspect ratio	[1-2]
warpage	[0-5]
angle quad (°)	[70-110]
angle tria (°)	[50-80]
Jacobien	[0.7-1]
% of trias	6

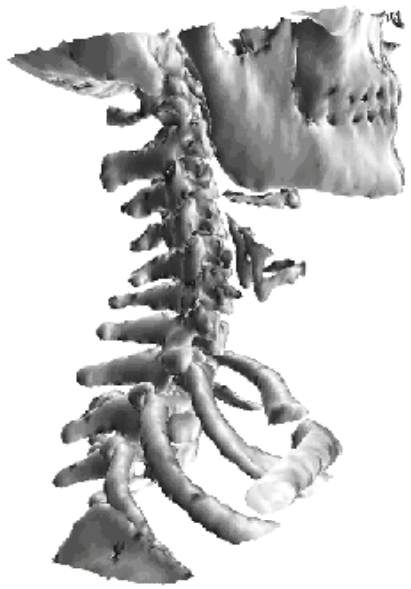

FIGURE 1. 3D reconstruction of the spine based on scanner sections in stereolithographic format.

The cervical vertebrae were modelled using shell elements, the intervertebral discs with brick elements, the ligaments using spring elements and finally the muscles as well as the soft tissues with brick elements. This choice of modelling may be justified as follows : For the cervical vertebrae, shell elements offer the possibility of strictly respecting the anatomical surface. This choice involves declaring this part as a rigid body in order to respect the geometry of the articular surfaces and to correctly reproduce the inertias. This simplifying hypothesis is not restrictive, however, insofar as the model is not interested to reproduce bone fractures, but to simulate more moderate lesions.

The modelling of the ligaments using spring elements means that parametric studies can easily be made both on stiffnesses and damping.

As far as the lower cervical spine is concerned, we have distinguished five types of ligaments : The anterior longitudinal ligament (ALL), the posterior longitudinal ligament (PLL), the flavum ligament (FL), the interspinal ligament (ISL) and finally the capsular ligaments (CL). This ligamentary system is shown in figure 2a.

For the upper cervical spine, we have modelled the posterior common ligament (C2-C0; C2-C1; C1-C0), the atloidien-axoidien anterior ligament, the transverse ligament, the yellow ligament (C2-C1), the transverse axoid ligament, the anterior occipito-atloid ligament, the alar ligament, the posterior occipito-atloidien ligament, capsular ligament C2-C1, capsular ligament Head-C1, membrane tectaria, the median occipito-odontoid ligament as well as the lateral occipito-atloidien ligament as illustrated in figure 2b.

Moreover, concerning the ligaments, we have deliberately introduced different numbers of springs for a given ligament out of a concern for biofaithfulness. The number of springs per ligaments is given in Appendix A.

The choice of modelling the intervertebral discs using volume elements in three layers was found to be indispensable to reproducing their behaviour correctly, given the 3D nature of this structure.

Finally, the soft tissues and the muscles are modelled using brick elements. This type of element offers the advantage of taking account of muscular mass, stiffness and the damping characteristics of this continuous medium. Particular attention was paid to the continuity of the meshing between the head, the cervical vertebrae and the muscles. Our will was to proceed a continuous meshing between the surface meshing (head and cervical spine) and the volume meshing (muscles and soft tissues). Therefore the only parts that are not in the continuous meshing are the articular process and the spinous process. Here, we placed an interface.

The finite element model of the head-neck system thus defined consists of 73 185 elements divided into 13 458 shell elements, 504 spring elements and 59.223 volume elements. A representation of this model is given in figures 3 and 4.

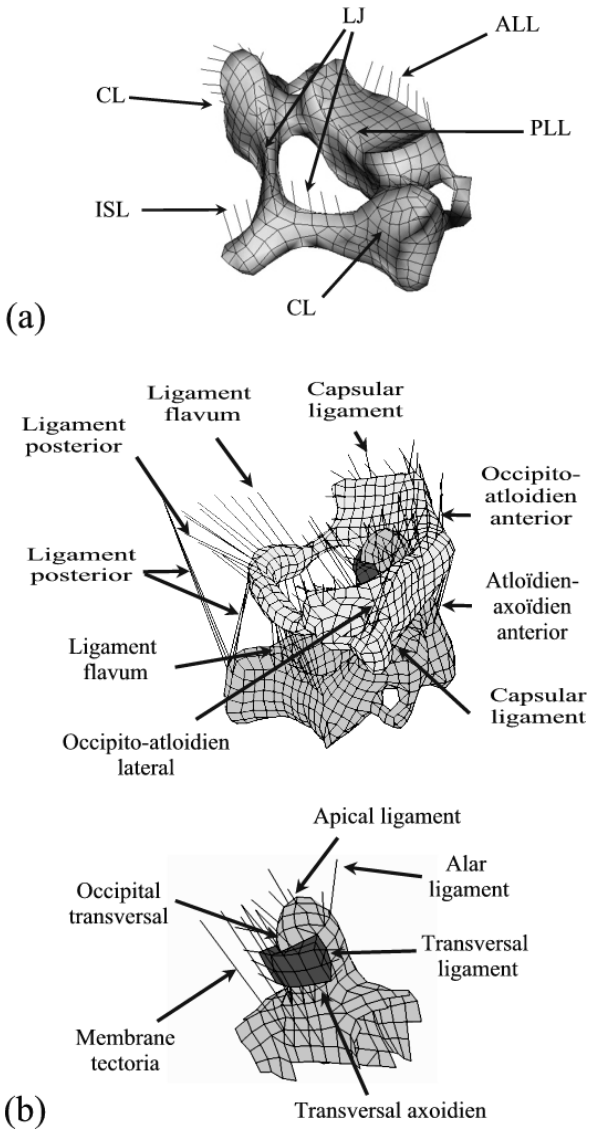

FIGURE 2. Ligamentary system of the lower cervical spine (a) and of the upper cervical spine (Atlas-Axis) (b).

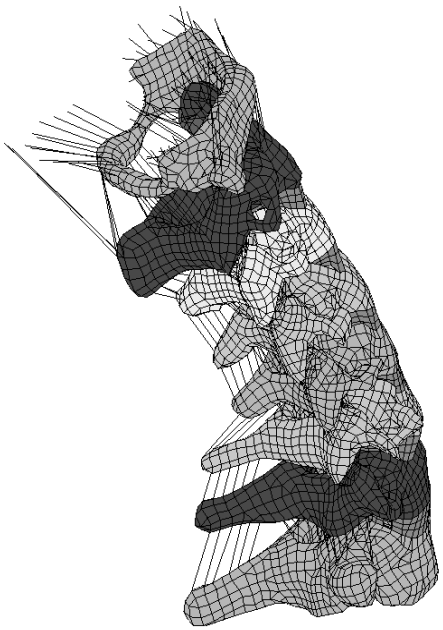

FIGURE 3. Surface meshing of the cervical column (C1-T1) with its ligamentary system.

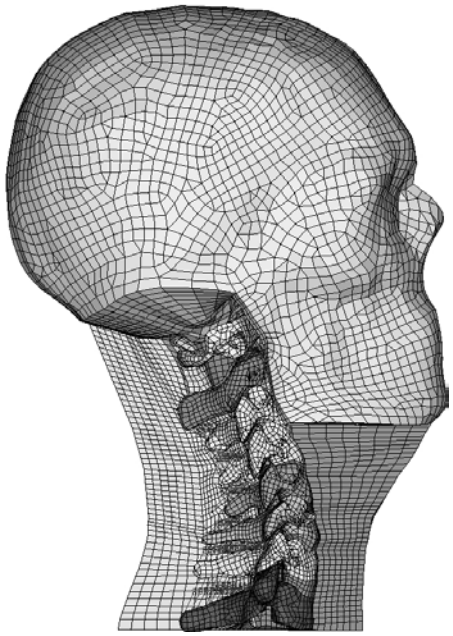

FIGURE 4. Complete finite element model of the head-neck system including modelling of the muscles using volume elements.

Mechanical properties

The ligaments were modelled using non-linear spring elements with a damping coefficient of η=900 Nm/s (De Jager et al. 1996, η=300Nm/s, Dauvilliers 1994, η=2000Nm/s). To define the behaviour laws of each ligament in both the lower and upper cervical spines, we referred to two complementary studies by Chazal et al. (1985) and Yoganandan et al. (2001). The Chazal et al. study (1985) highlights the non-linear viscoelastic behaviour of ligaments whereas Yoganandan et al. (2001) gives information on their failure properties. The overall behaviour of the ligaments can then be characterised by three pairs of coefficients α_1, α_2, α_3 determining the zone of low rigidity or neutral zone, the linear part, and finally the plastic behaviour. The coefficients used for our model are described in Table 2 and a representation of the typical behaviour of the five ligaments of the lower cervical spine is illustrated in figure 5.

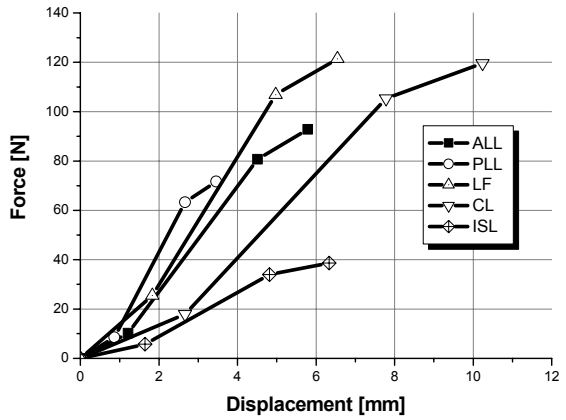

FIGURE 5. Behaviour laws of the anterior longitudinal ligaments, ligament (ALL C2-C5), posterior longitudinal ligament (PLL C2-C5), flaval ligament (FL C2-C5), interspinous ligament (ISL C2-C5), capsular ligament (CL C2-C5). Yoganandan et al. (2001) and Chazal et al. (1985).

In order to take into account the initial lengths of the ligaments in the model as well as those measured anatomically by Yoganandan et al. on the lower cervical spine (2001) we calculated the laws as follows :

$$\begin{cases} d_i = \alpha_i * L * \left(\dfrac{L_m}{L} \right) \\ F_i = \dfrac{F_3 * \alpha_i}{N_{spring}} * \left(\dfrac{L_m}{L} \right) \end{cases} \qquad i = 1,2,3 \qquad (1)$$

with d_i is the spring elongation, F_i the force, N_{spring} number of springs, L the experimental ligament length and L_m the mean length spring in the model.

For the upper ligaments the initial experimental lengths are not given by Yoganandan et al. (2001), so the ratio between the initial length of the model and experimental are equal to 1.

All the mechanical properties of the ligaments are detailed in the summary table in Appendix A.

Intervertebral disks have been poorly studied. Moroney et al. (1988) have measured a value of 500 MPa for compression solicitations. Yoganandan et al. (2001) have measured a Young modulus of elasticity for the anulus ground substance ranged from 3.4 to 4.7 MPa , and a linear Young modulus of 450 to 500 MPa for the anulus fibers.

In our model the hypothesis of a homogeneous linear elastic isotrope material was considered with a Young modulus of 100 Mpa and a Poisson's ratio of 0.3. These values are situated between the extreme values related in the literature which represents a global behaviour of this structure (Kleinberger (1993), Dauvilliers (1994)).

The cervical vertebrae were declared as rigid bodies. The mechanical characteristics in terms of masse and inertias are taken from the work of Deng et al. (1987) and detailed in Table 3.

A passive law (Eq.2) has been set to model the muscle behaviour. This law was taken from the work of Knudsen (1953).

$$\sigma = \frac{E_0}{\alpha}\left(e^{\alpha\varepsilon} - 1 \right) \qquad (2)$$

The Young Modulus E_0 was calibrated with the Myers et al. experimental data (1995) and set to 0.15 Mpa and α set to 1.

For the anterior muscles an elastic law was applied. The Young modulus is E=0.05 Mpa and the Poisson's ratio is set to 0.4.

TABLE 2. Coefficients used to define the ligaments constitutive laws (Chazal et al. 1985). The rupture strengths are taken from Yoganadan et al. (2001). For remaining data see Appendix A.

	α_1		α_2		α_3			
Ligament	$\varepsilon_1/\varepsilon_{3max}$	F_1/F_{3max}	$\varepsilon_2/\varepsilon_{max}$	F_2/F_{3max}	ε_{3max} C2-C5	F_{3max} C2-C5	ε_{3max} C5-T1	F_{3max} C5-T1
ALL	0.21	0.11	0.78	0.87	0.308	92.8	0.354	145.2
PLL	0.25	0.12	0.77	0.89	0.182	71.1	0.341	188.2
FL	0.28	0.21	0.76	0.88	0.77	121.5	0.884	129.1
ISL	0.3	0.17	0.75	0.87	0.609	38.6	0.681	38.6
CL	0.26	0.15	0.76	0.88	1.41	119.7	1.16	181.1
Average for the upper cervical spine	0.26	0.15	0.76	0.88	1	-	1	-

TABLE 3. Inertial properties of the cervical vertebrae and head applied to the centres of gravity.

Name	***Mass [Kg]***	***Ixx [Kg.m²]***	***Iyy [Kg.m²]***	***Izz [Kg.m²]***
T1	-	-	-	-
C7	0.22	2.2	2.2	4.3
C6	0.24	2.4	2.4	4.7
C5	0.23	2.3	2.3	4.5
C4	0.23	2.3	2.3	4.4
C3	0.24	2.4	2.4	4.6
C2	0.25	2.5	2.5	4.8
C1	0.22	2.2	2.2	4.2
Head	4.69	181	236	173

Temporal validation of the finite element model

A temporal validation of the new model has been carried out in comparison to the N.B.D.L tests (Ewing 1968) with front, oblique and lateral impacts as well as a rear impact validation based on Prasad's tests on cadavers (1997). This temporal analysis allows us to validate the model in accordance with the classic validation procedures systematically chosen in the literature (Dauvilliers (1994), de Jager (1996), Astori et al. (1998)). The advantage of the N.B.D.L tests is that they are well instrumented tests carried out on volunteers and quite violent (15g for 100 ms). First of all, they constitute an interesting source of validation of the head kinematics. Of course, the same mechanical properties of the model were retained for the four impact simulations. The imposed speeds at T1 are given in figures 6 to 9. The evaluation of the model is then obtained by superposing the acceleration and the displacement of the anatomical centre of the head (AC). In figures 10 through 13 we report the results obtained with the four impact configurations (front, rear, oblique and lateral). In order to compare the response of the model with the experimental data, a quantitative analysis was carried out for the four impacts (frontal, rear, oblique and lateral). Each curves were sampled at 2000 Hz like the experimental data. This statistical method consists then to determine the number of points at the interior of the experimental corridor. The values obtained in term of percentage are given in appendix C.

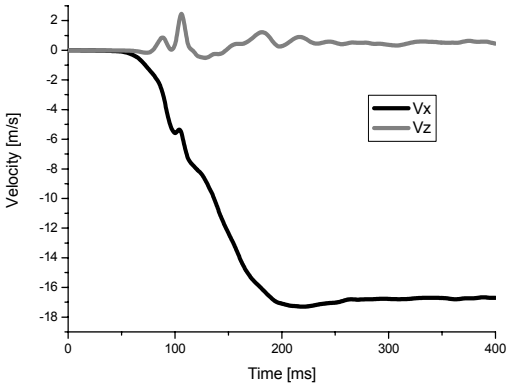

FIGURE 6. Imposed speed at T1 in the case of a front impact.

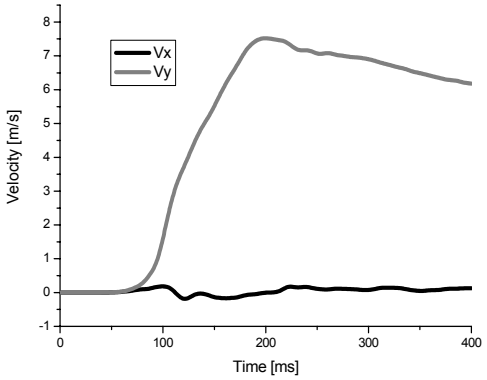

FIGURE 7. Imposed speed at T1 in the case of a lateral impact.

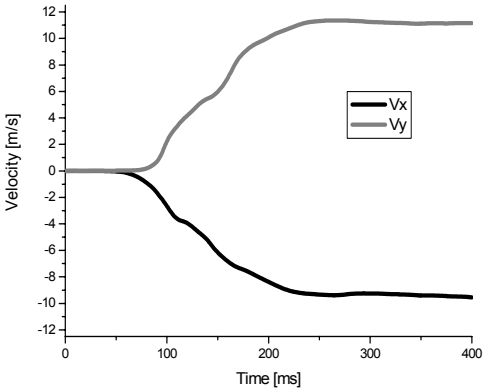

FIGURE 8. Imposed speed at T1 in the case of an oblique impact.

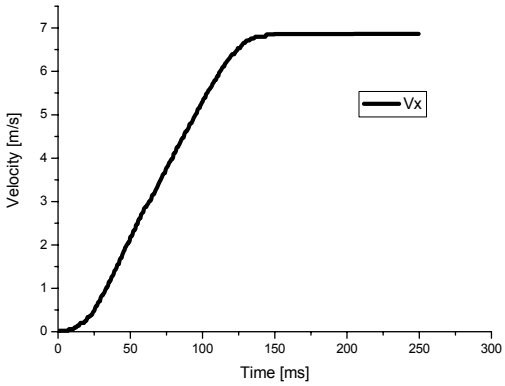

FIGURE 9. Imposed speed at T1 in the case of a rear impact.

Frontal impact. Figures 10a to 10f show the response of the finite element model comparing to the volunteers in terms of accelerations, displacement and rotation.

We can observe in figure 10b a good correlation in terms of y-angular acceleration (74.3%).

55% of the response in terms of linear accelerations is include in the experimental corridor (figure 10a and 10c). In addition, the model correctly reproduces displacement along X-axis to 67.9% (figure 10d). One can nevertheless observe that displacement along Z-axis is underestimated (9%) as illustrated in figure 10f.

The details of the statistics results is presented in table C1 (Appendix C)

The view shown in figure 10g illustrates realistic kinematics with regard to the inclination of the column.

(a)

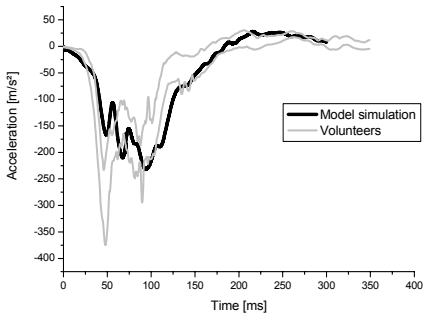

(d)

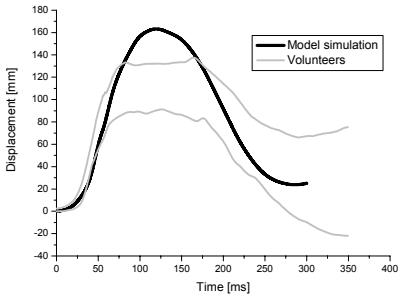

(b)

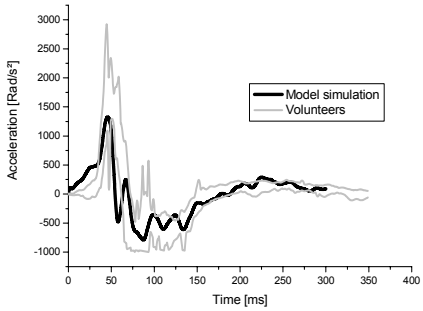

(e)

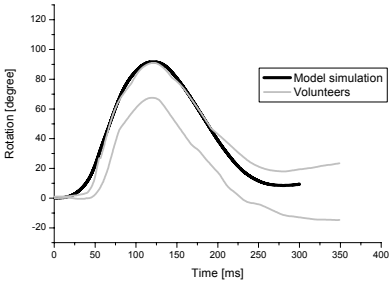

(c)

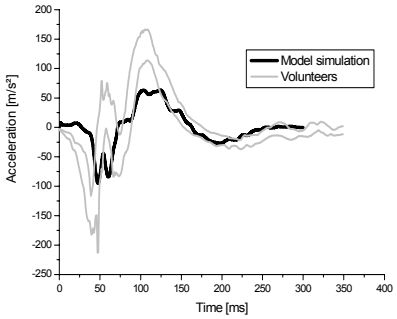

(f)

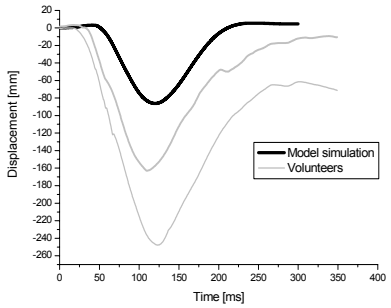

(g)

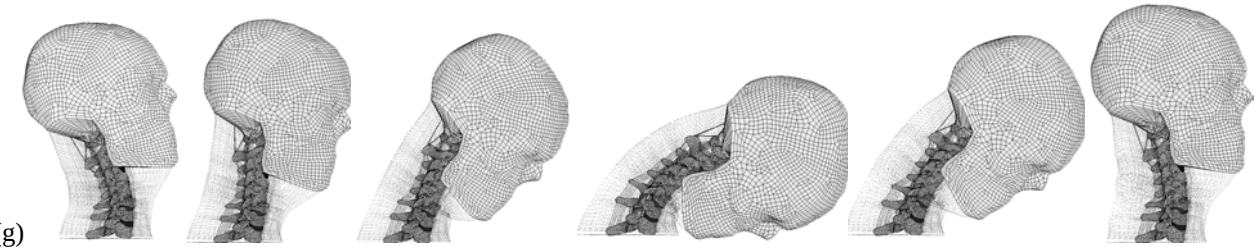

Time = 0 ms Time = 50 ms Time = 70 ms Time = 120 ms Time = 170 ms Time = 300 ms

FIGURE 10. Results of the frontal impact : (a) X-axis linear acceleration of the anatomical centre (AC) of the head, (b) Y-axis angular acceleration of the AC, (c) Z-axis linear acceleration of the AC, (d) X-axis displacement of the AC, (e) Rotation of the AC, (f) Z-axis displacement of the AC and (g) Kinematic response of the finite element model to a frontal impact (N.B.D.L., Ewings et al. 1968, 1977).

Rear impact. This validation, less well instrumented than that carried out by the N.B.D.L, nevertheless allows us to estimate the behavior of the model during a rear impact. Figures 11a to 11e compare the model and the cadaver responses in terms of accelerations, displacement and rotation of the AC. The FEM correctly reproduces rotation along the Y-axis (100%), displacement of the centre of gravity of the head following Z-axis (70.2%) as well as the angular acceleration along the axis Y (60.3%).

However, only 5.8% of the points calculated concerning displacement along axis X is inside the corridor (figure 10c). All results are given in table C4 (Appendix C). The configuration of the finite element model for the rear impact is shown in figure 11f.

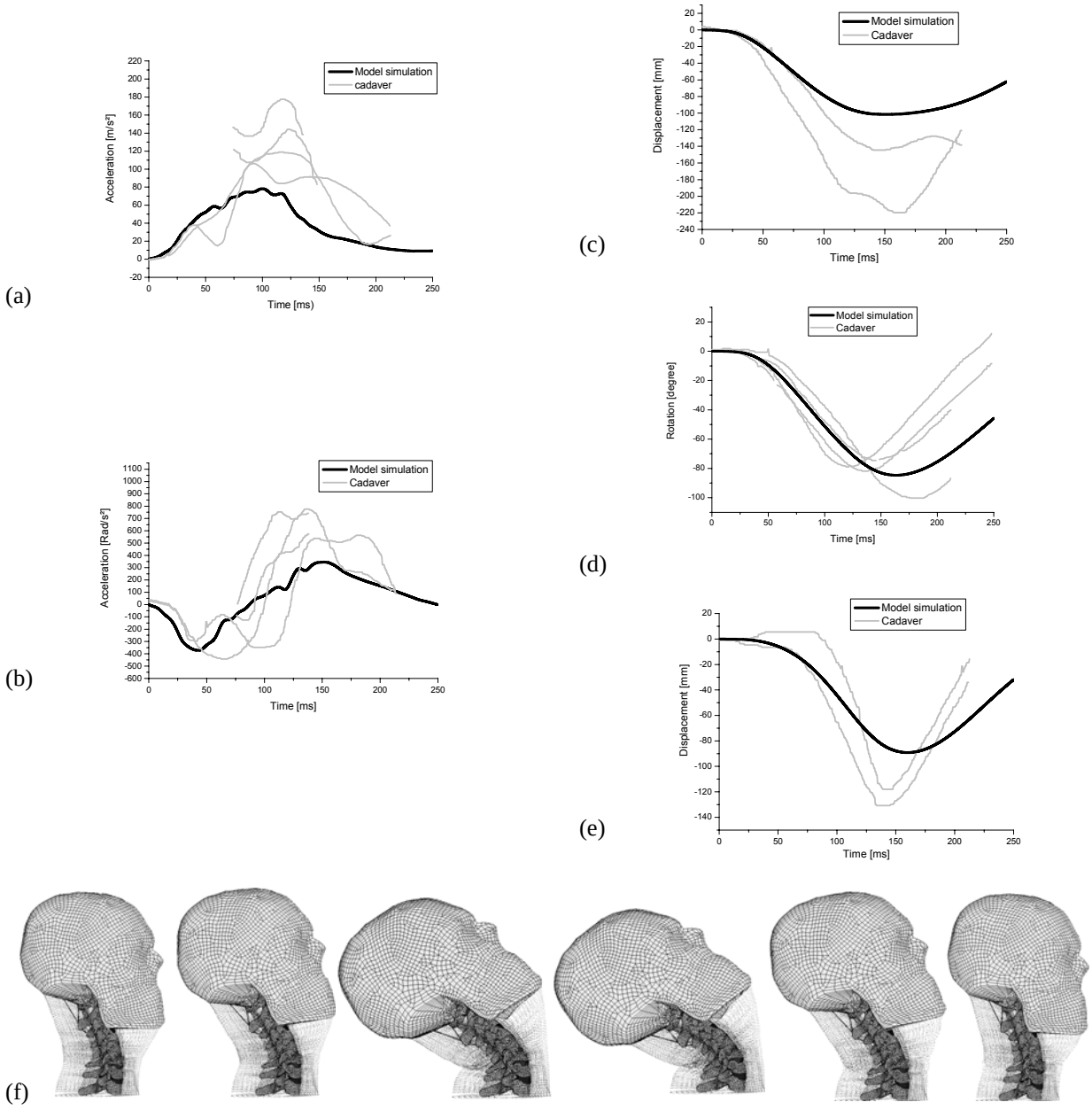

FIGURE 11. Results of a rear impact : (a) Resultant acceleration of the AC, (b) angular acceleration of the AC., (c) X-axis displacement of the AC, (d) Rotation of the AC, (e) Z-axis displacement of the AC and (f) Kinematic response of the finite element model to a rear impact (Prasad et al. 1997).

Oblique impact. Kinematics' response under an oblique impact is very close to that of the volunteers throughout the duration of the impact (66%, table C3 Appendix C). Only the z-axis displacement is slightly underestimated (27.3%) as illustrated in figure 12l.

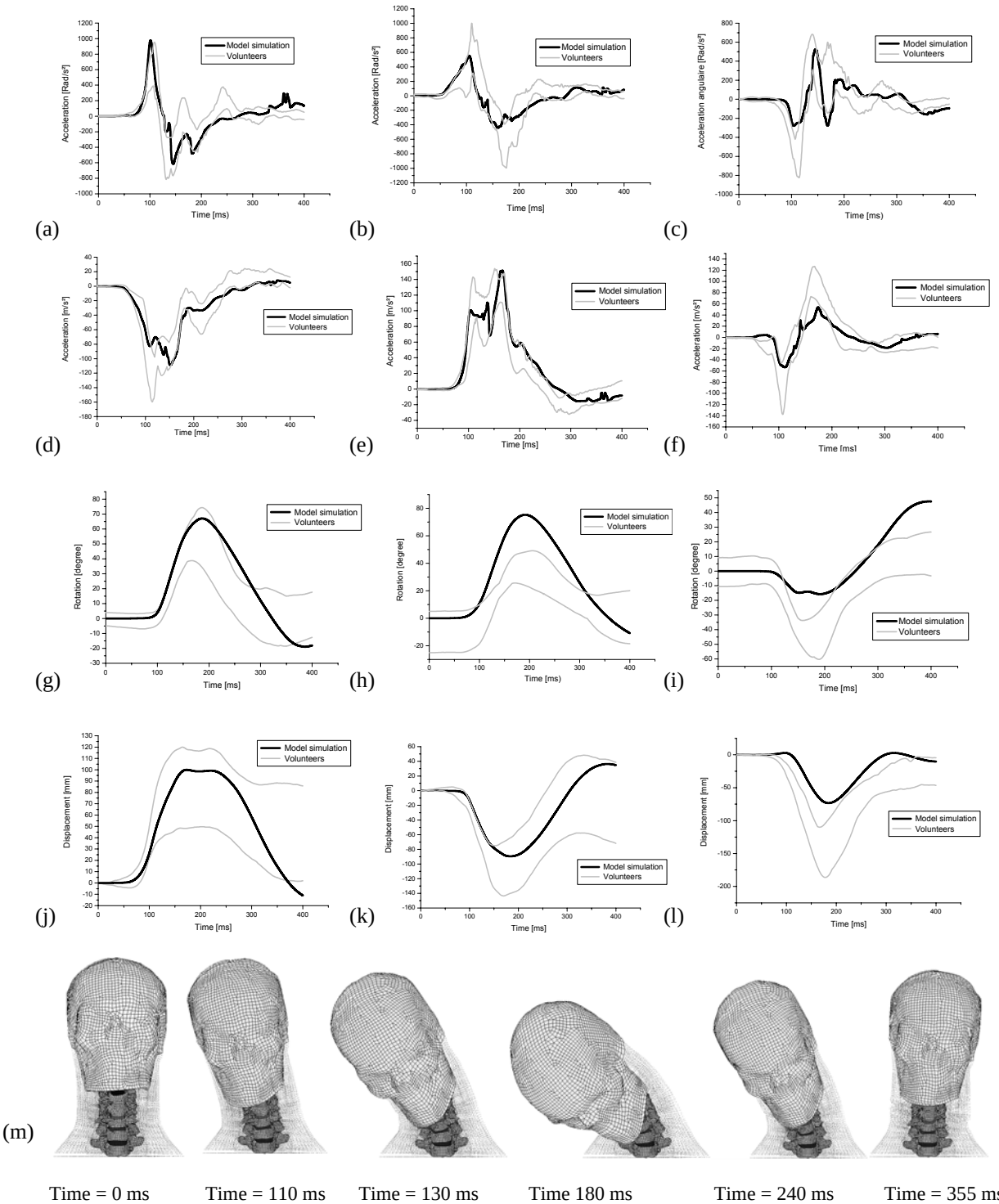

FIGURE 12. Results of an oblique impact : X-axis (a), y-axis (b) and z-axis (c) angular accelerations of the AC respectively, X-axis (d), y-axis (e) and z-axis (f) linear accelerations of the AC respectively, X-axis (g), y-axis (h) and z-axis (i) rotation of the AC respectively, X-axis (j), y-axis (k) and z-axis (l) displacement of the AC respectively and (m) Kinematic response of the finite element model to an oblique impact (N.B.D.L., Ewings et al. 1968, 1977).

Lateral impact. In the same way as for the oblique impact configuration, there is globally a good correlation between the FEM and the volunteers throughout the duration of the impact (73.3%) as it can be observed in figure 13 and calculated in table C2 (Appendix C).

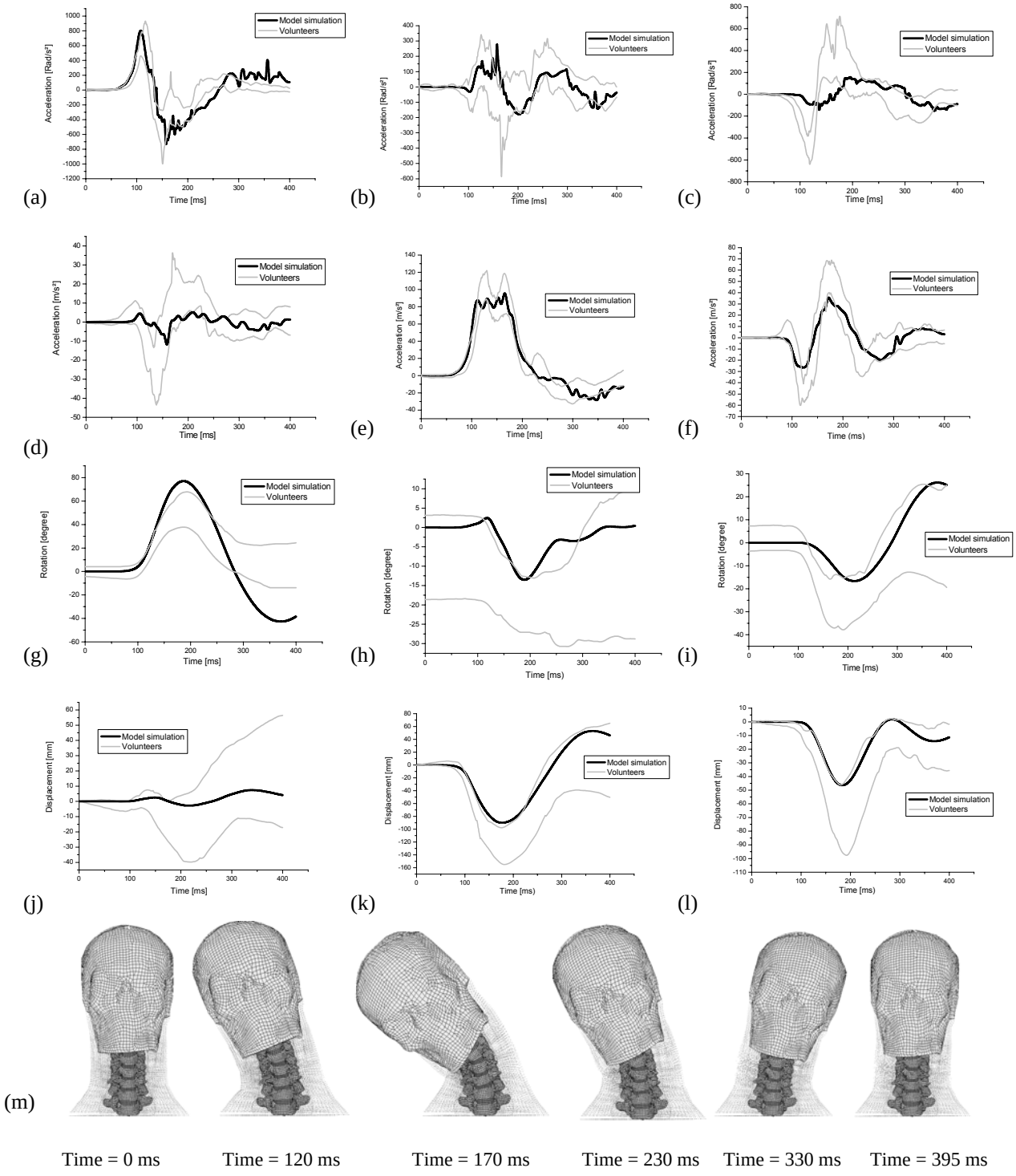

FIGURE 13. Results of a lateral impact : X-axis (a), y-axis (b) and z-axis (c) angular accelerations of the AC respectively, X-axis (d), y-axis (e) and z-axis (f) linear accelerations of the AC respectively, X-axis (g), y-axis (h) and z-axis (i) rotation of the AC respectively, X-axis (j), y-axis (k) and z-axis (l) displacement of the AC respectively and (m) Kinematic response of the finite element model to a lateral impact (N.B.D.L., Ewings et al. 1968, 1977).

In view of these results, it is commonly accepted that the model correctly reproduces the behaviour of the head-neck system in spite of the wide corridors which allow non-significant acceleration peaks or inclines. Figure 14 clearly illustrates that these "corridor validations" allow an FEM to have several fundamentally different responses that absolutely do not translate the behaviour. It is, however, impossible in the temporal domain to analyse what mechanical significance they represent.

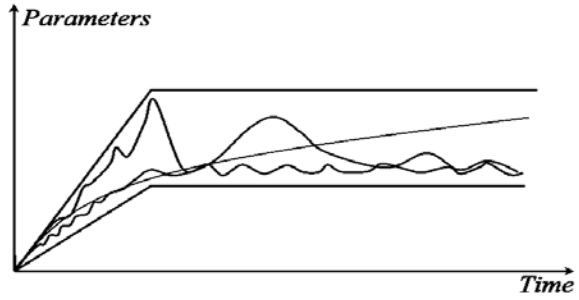

FIGURE 14. Example of three different dynamic responses, all of them acceptable within a corridor.

Experimental modal analysis of the head neck system

In this section, modal characterization of the head-neck system in vivo is described for five healthy volunteers (25-48 years) without cervical disease[2]. All subjects underwent a medical check prior to the experiments, and were asked if any symptoms of any kind have appeared after the experiments. None of them complained any discomfort.

The experimental device, represented in figure 15, consists on a pendulum (length of 0.5 m) articulated on a gantry which impacted frontally the volunteers' forehead with a basketball. The mass of the impactor is about 3.6 kg and the angular displacement of 20° can produce an impulsive force of 60 N to 150 N and head accelerations of 2g to 3g. The volunteer is seated on a rigid seat without headrest. His shoulders are strongly maintained against the backrest of the seat in order to avoid the contribution of the torso movement. In this experimental configuration, the volunteers have been asked to close eyes and to have the muscles of the neck relaxed during the entire test, in order to avoid the muscles contribution. It is hypothesized that the head motion remains in the sagittal plan with an amplitude sufficiently small (a few degrees) that the applied frontal force and the recorded linear acceleration can be assumed as unidirectional in the antero-posterior direction. The head acceleration is measured using nine accelerometers (Entran EGA ±10 g) arranged in the well-known 3-2-2-2 (figure 16) in order to calculate the linear component of the head acceleration at vertex and at atlanto-occipital joint. The impulsive force is recorded using a force sensor (PCB 208A02 11.432 mV/N).

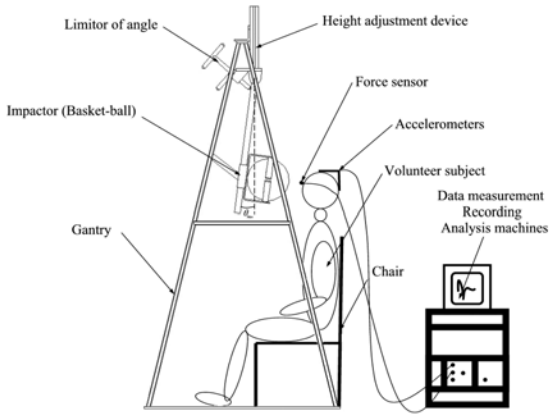

FIGURE 15. Experimental test device for the modal analysis of the head neck system.

FIGURE 16. Detail of the 3D accelerometer setup fitted to the volunteer's head.

Force and acceleration signals are digitised via a National Instrument (NI) data acquisition and signal conditioning is provided with a PXI-6070E 12 bit card. Signal acquisition is performed under LabView (NI) program and data processing is written using Matlab software. Antero-posterior linear accelerations are calculated at the vertex level (point

[2] The experimentation being non invasive and done within normal human physiological limits (the impacts to the head being largely under tolerance limits) our methodology was conducted in accordance with the practice of the responsible governing authority as described by *the Ethics Committee of the French Centre National de Recherche Scientifique (CNRS)*.

S) as well as at the atlas to occipital jonction point O_H, as illustrated in figure 17.

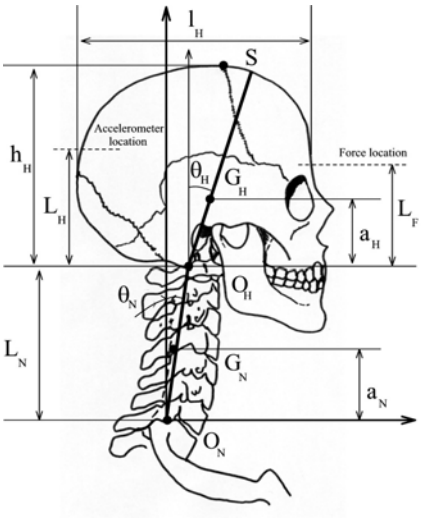

FIGURE 17. Representation of the head-neck system in the sagittal plan.

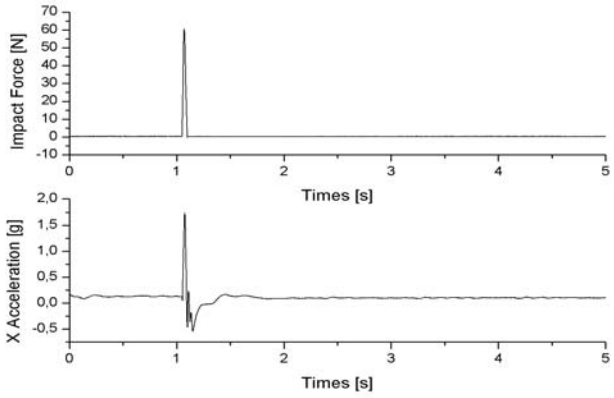

FIGURE 18. Temporal evolution of applied force and linear acceleration response calculated at vertex level.

Figure 18 illustrates the temporal signals of force input and acceleration output at vertex level. After impact, the transfer function between force and point S acceleration is estimated in terms of apparent mass. Special attention has been paid to the management of noise, as well as the checking of linearity, ergodicity and the stationary nature of the signals.

In order to minimize noise linked to the digitizing effects, the Standard Normalized Error is calculated by repeating each experiment ten times for each volunteer. The estimated transfer function and the standard deviation can then be calculated with a 95% confidence. However, the first step is to check the linearity of the head-neck system by figuring the coherence function between the input force signal ($x(t)$) and the output acceleration signal ($y(t)$). The equation of the coherence function can be written as :

$$\hat{\gamma}^2_{xy}(w) = \frac{\left|G_{YX}(w)\right|^2}{G_{YY}(w).G_{XX}(w)} \qquad (3)$$

Where G_{XX}, G_{YY} and G_{XY} are the autospectrums and interspectrum of the signals obtained in the frequency domain (Bendat et al. 1971).

The linearity of the system is generally accepted if the coherence function remains between 0.9 and 1 in the analysed frequency range. The response signal contains not only the response due to the measured excitation, but also the response due to the ambient random excitation. We can therefore characterize this typical measurement as having noise in the measured output signal. Using the principle of least squares, to minimize the effect of noise at the output, the best Frequency Response Function (FRF) estimator is :

$$\hat{H}(w) = \frac{G_{XY}(w)}{G_{XX}(w)} = \left|\hat{H}(w)\right|.e^{-j\hat{\Phi}_1(w)} \qquad (4)$$

Accordingly, the transfer function between force and accelerations have been calculated in terms of apparent mass by using equation (4) for a total of five volunteers. The five subjects are all males with different masses and sizes. Figure 20a represents the average of the five transfer functions between force and point S acceleration with their standard deviations. Figure 20b shows that the coherence functions are close to 1 in the analysed frequency range, which proves the linear behaviour of the head-neck system under the conditions of the study.

All the subjects present a similar frequency response characterized by two natural frequencies : the first mode at 1.3 ± 0.1 Hz and the second mode at 8 ± 0.7 Hz. The transfer function between atlanto-occipital junction and force for all subjects was calculated but not reported. Therefore the simplest model which can simulate this transfer function is a two mass system connected with a set of springs and dashpots. This is provided by the classical two pivots neck model. This two pivots model is justified by the studies of Wen and Lavaste (1993a and 1993b) which explain the main mobilities of the head-neck system are located at the C7-T1 jonction and the atlanto-occipital joint.

A single punctual transfer function between acceleration at vertex and the input force at forehead cannot contain all information relating to a system with two degrees of freedom. A second transfer

function is needed in order to extract the mode shape relating to each identified natural frequency. The horizontal linear acceleration at atlanto-occipital joint (point O_H) is selected for this purpose and the transfer function between this parameter and the input force is established in a way similar to the transfer function between point S acceleration and force. We have represented the transfer function in terms of apparent mass for each volunteer and tabulated the frequencies responses in figure 19. The mode shapes obtained with the imaginary part of the dynamic stiffness, are drawn in figure 21a and the extracted eigenvector are shown in figure 21b where we can observe clearly that the first mode at 1.3 ± 0.1 Hz is an extension mode and the second mode at 8 ± 0.7 Hz a retraction mode (figure 21c). It can be remarked that the standard deviation on natural frequencies obtained for the five volunteers is very low for the biomechanical domain as stipulated in Table 4 (15% for the first natural frequency and 17.5 % for the second natural frequency). In figure 20, the error on the modulus and phase is explained by the inter-subject variability (head and neck masses, length, etc.). These results constitute new validation parameters for the following FE model validation in the frequency domain.

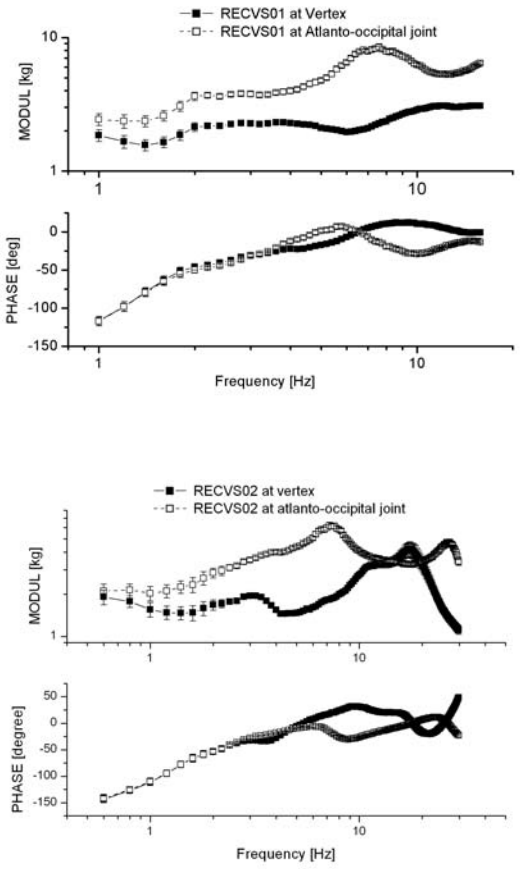

FIGURE 19. Representation of the five apparent mass at vertex and at atlanto-occipital joint.

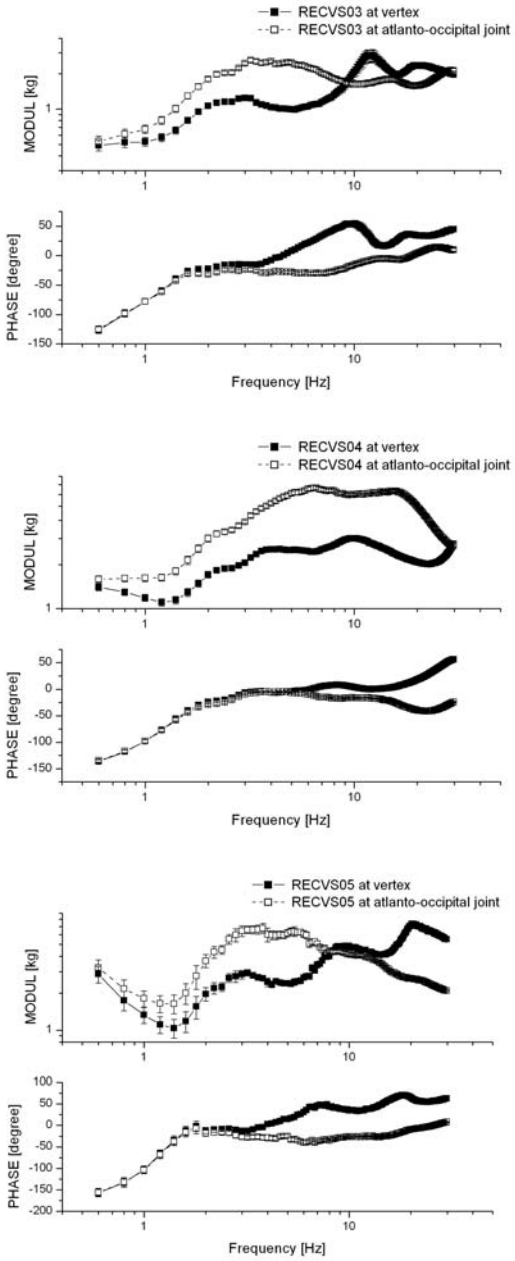

Table 4 : Eigenfrequencies of the five volunteers and the average.

	Mode 1	***Mode 2***
RECVS01	1.4 Hz	8.8 Hz
RECVS02	1.7 Hz	8.3 Hz
RECVS03	1 Hz	7.8 Hz
RECVS04	1.2 Hz	8.4 Hz
RECVS01	1.2 Hz	6.9 Hz
Means	1.3±0.1 Hz	8±0.7 Hz
Errors	**15 %**	**17.5 %**

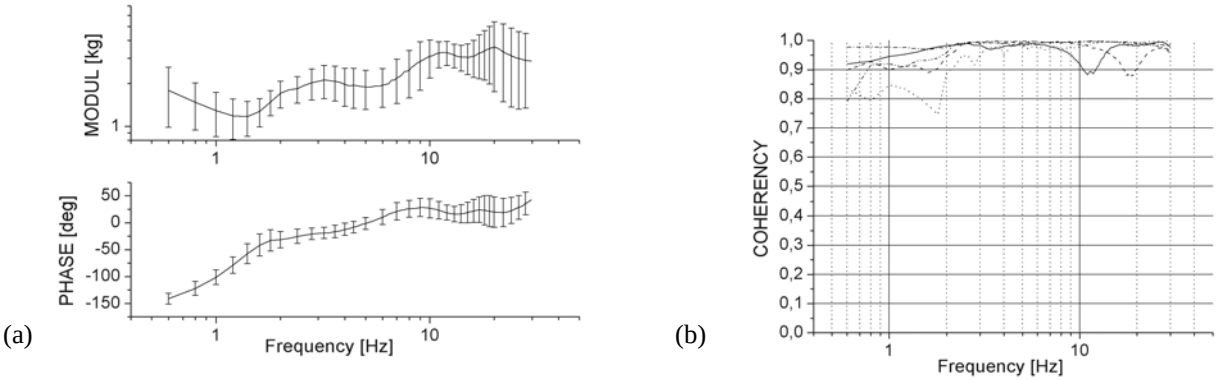

(a) (b)

FIGURE 20. (a) Average of the five transfer functions between vertex acceleration and force, and (b) Coherence function.

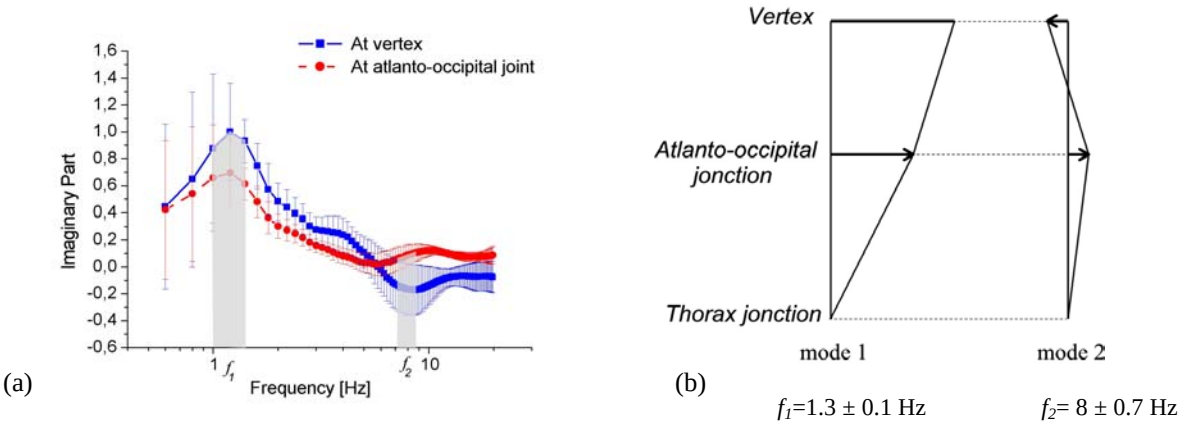

(a) (b)

f_1=1.3 ± 0.1 Hz f_2= 8 ± 0.7 Hz

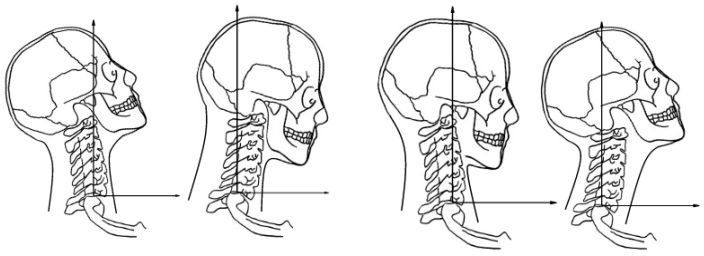

(c)

Shape 1 Shape 2

f_1= 1.3 ± 0.1 Hz f_2 = 8 ± 0.7 Hz

FIGURE 21. (a) Imaginary part of the two transfer fonctions intended to extract the two mode shapes (b).(c) Representation of the two mode shapes, Shape 1 is an flexion-extension mode at 1.3 Hz and shape 2 is the anterior-posterior retraction of the neck at 8 Hz.

RESULTS

Numerical modal analysis of the head-neck system

The above descript experimental modal analysis was performed numerically by simulating the experience with the head-neck FE model followed by a results analysis in the frequency domain as illustrated in figure 22. The experimental results presented in this modal analysis correspond to the response of the subject modelled (RECVS01). We assumed that the first thoracic vertebra was fixed and reproduced the impact load in its amplitude and duration. To simulate the force of the impact between the ball and the head a Young's modulus of E=0.3 Mpa (ν=0.49) was implemented for the modelling of the ball and an initial horizontal speed of 0.6 m/s. The acceleration at the vertex and at the occipital joint was computed over 5 s.

The superposition of the experimental and digital curves in terms of force and acceleration is illustrated in figure 23b. The conformity of the simulation with the experiment is based on the ball-head interaction force 23a.

(a)

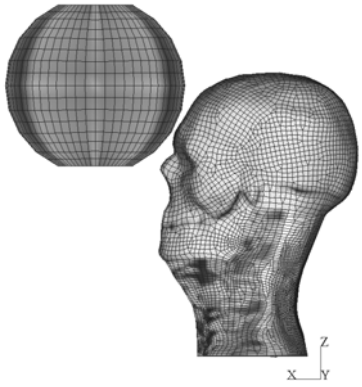

(b)

FIGURE 22. (a) Experimental configuration of the experimental modal analysis, and numerical replication with the finite element model of the neck (b).

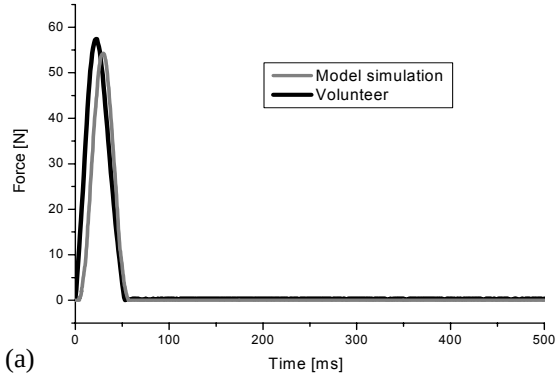

(a)

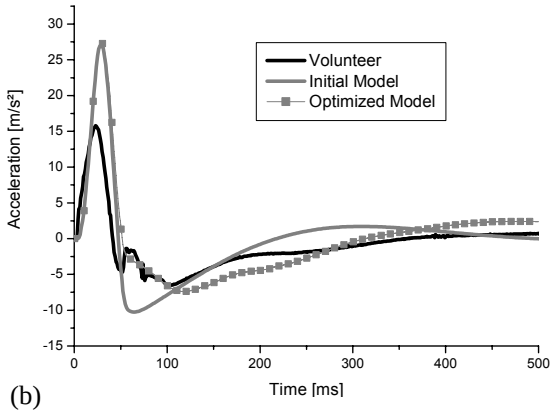

(b)

FIGURE 23. (a) Experimental and digital interaction force between the head and the ball and (b) acceleration curves for the head at the vertex.

After calculation of the acceleration at the vertex and at the atlanto-occipital joint the same signal processing is carried out as in the experimental tests between the force and the acceleration (Matlab software). In order to analyse the frequency response of the model, we therefore expressed the amplitude in terms of apparent mass amplitude, phase and imaginary part.

According to the amplitude of the apparent mass, reported in figure 24, we are able to assert that model does not faithfully reproduce the behaviour of the head-neck system. This frequency response establishes that the model reproduces more or less correctly the first mode, namely flexion-extension at a natural frequency of 2.8 Hz as against 1.4. Hz for the volunteer. On the other hand, as far as the second mode is concerned, namely the retraction of the neck or the translation of the head, the calculation shows

that the model has a natural frequency of 40 Hz as against 8.8 Hz in-vivo as illustrated with the imaginary part in figure 25. This poor result can be explained by the fact that the temporal validation, under front and rear impacts, focused on the flexion-extension motion of the head and less on its translation. This latter motion is in fact much more difficult to analyse from the temporal data at the very beginning of the impact. It is therefore understandable that the modal behaviour of the neck FE model is realistic for extension motion of the head (100% error), but reproduces very badly the second mode relating to retraction (350% error).

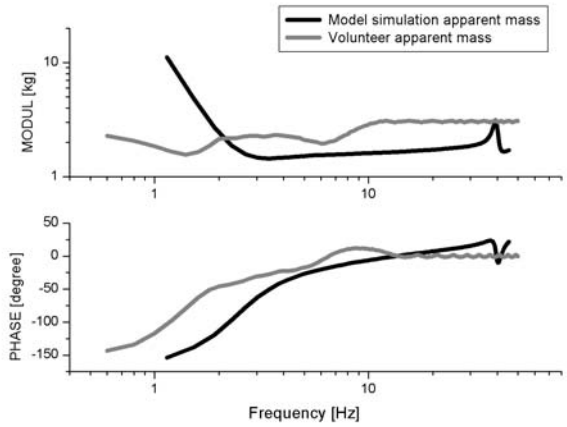

FIGURE 24. Apparent mass and of the neck FEM with the identical mechanical properties as during the multidirectional temporal validation superimposed to the volonteer one.

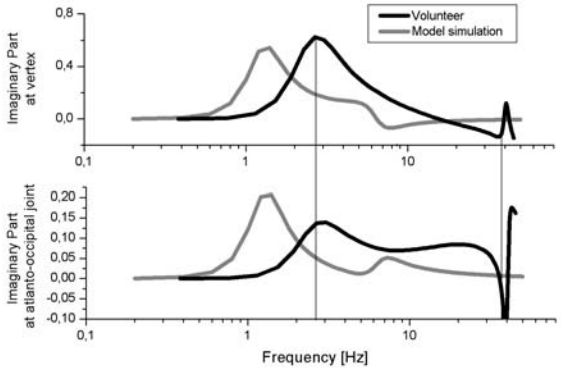

FIGURE 25. Superimposition of the numerical and volunteer imaginary part of the transfer function at the vertex and atlanto-occipital junction. It appears clearly that the second natural frequency is over estimated by the model.

Moreover, in view of the apparent mass, we can see that the amplitudes are clearly too low, which expresses a too high a damping of the ligaments and in particular in the upper cervical spine. It should be noted that the ligament damping is open to discussion in the FEM of the neck for the simple reason that no experimental data are available. In the literature it is the overall trajectory of the model during an impact that serves to adjust the value of this damping.

In order to reproduce a realistic modal behaviour of the neck FEM, characterised by the two natural frequencies (1.4 Hz and 8.8 Hz) of the RECVS01 volunteer , a parametric study concerning the rigidity as well as the dumping has been performed. It appeared that the model whose frequency behaviour comes closest to that of the volunteer is obtained with a reduction in the rigidity of the upper ligaments of 20% with a damping of 9 Nm/s against 900 Nm/s for the initial model, and a damping of the lower ligaments remaining at 900 Nm/s. The apparent mass of the optimised model is superposed with that of the volunteer in figure 26.

In spite of a difference between the model and the volunteer, the frequency response of the model presents resonance frequencies very close to the volunteer. So, after optimisation the calculated values obtained from our FEM were f_1=1.6Hz (against 1.4Hz) and f_2=8Hz (against 8.8Hz) respectively corresponding to a 14% difference in the first mode and a 9% difference in the second mode.

This result demonstrates the importance of the mechanical properties of the ligaments and in particular their damping coefficients, which have a major influence on the resonance frequencies as well as on the volunteer's apparent mass amplitude. As the signals recorded during the temporal validation are too complex, it is quasi-impossible to observe the influence of these parameters on the retraction phenomenon. Only a modal analysis will finally have allowed us to adjust this parameter in a realistic way. However, we can observe in figure 27, in view of the imaginary part at the head-neck junction, that the amplitude is still too low, which expresses a slightly too low flexion motion possibly due to approximation in head mass and inertia estimation.

.

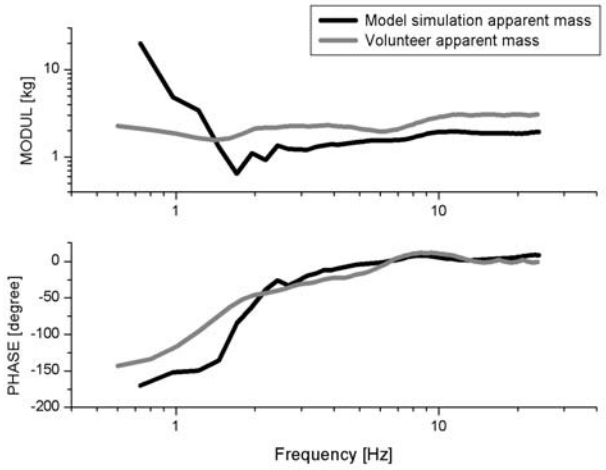

FIGURE 26. Apparent mass and of the optimise neck FEM superimposed to the volonteer one.

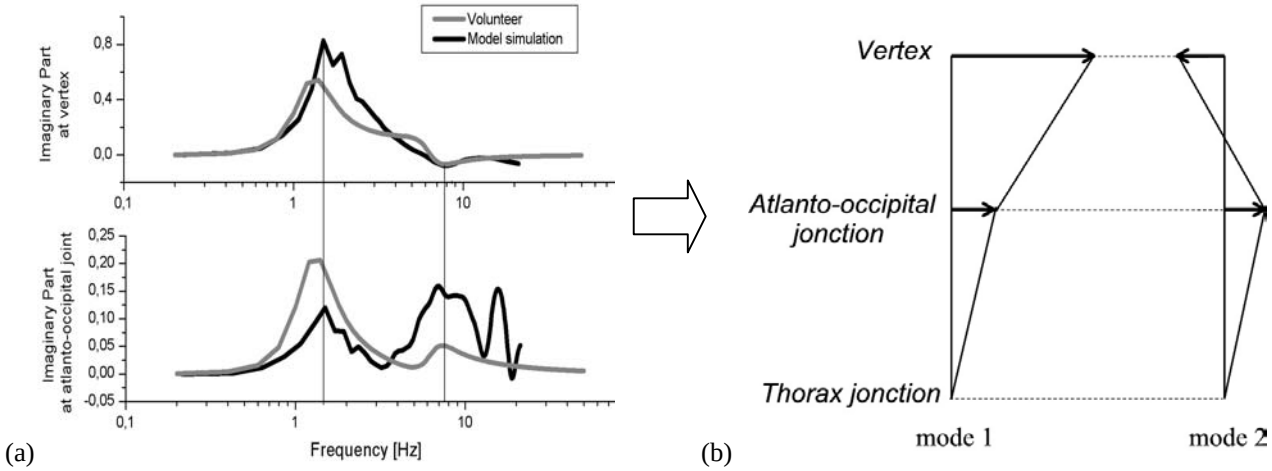

FIGURE 27. (a) Superimposition of the numerical and volunteer imaginary part of the transfer function at the vertex and atlanto-occipital junction after the neck FEM optimisation. (b) Representation of the two mode shapes, Shape 1 is an flexion-extension mode at 1.6 Hz and shape 2 is the anterior-posterior retraction of the neck at 8 Hz

The modal analysis being restricted to the linear domain, the optimised model was finally confronted with a classic validation in the temporal domain by the simulation of the four impacts simulated earlier with the initial mechanical properties. The goal of this study was not to fit the temporal response but to demonstrate the compatibility of a frequency approach and temporal approach. The results of this temporal domain check of the frequency optimised model are reported in figures 28 to 31. Statistical values have been calculated in Appendix C.

For the frontal impact, only the displacement in the z plane is slightly underestimated (26% against 9% for the initial model) as illustrated in figure 28f. Globally, 45.6% of the FEM response is in the experimental corridor Concerning the rear impact, responses of the FEM are lower than cadavers for x-displacement (36.9%) and higher for y-rotation (50%). In addition for the oblique impact the globally response of the model is very similar to the volunteers as illustrated in figure 30 with 62.1%. Finally for the lateral impact there is a good correlation between the model and the volunteers with a statistical value about 73.3% (figure 31).

Temporal results of the neck FEM during the frontal impact after its frequency validation.

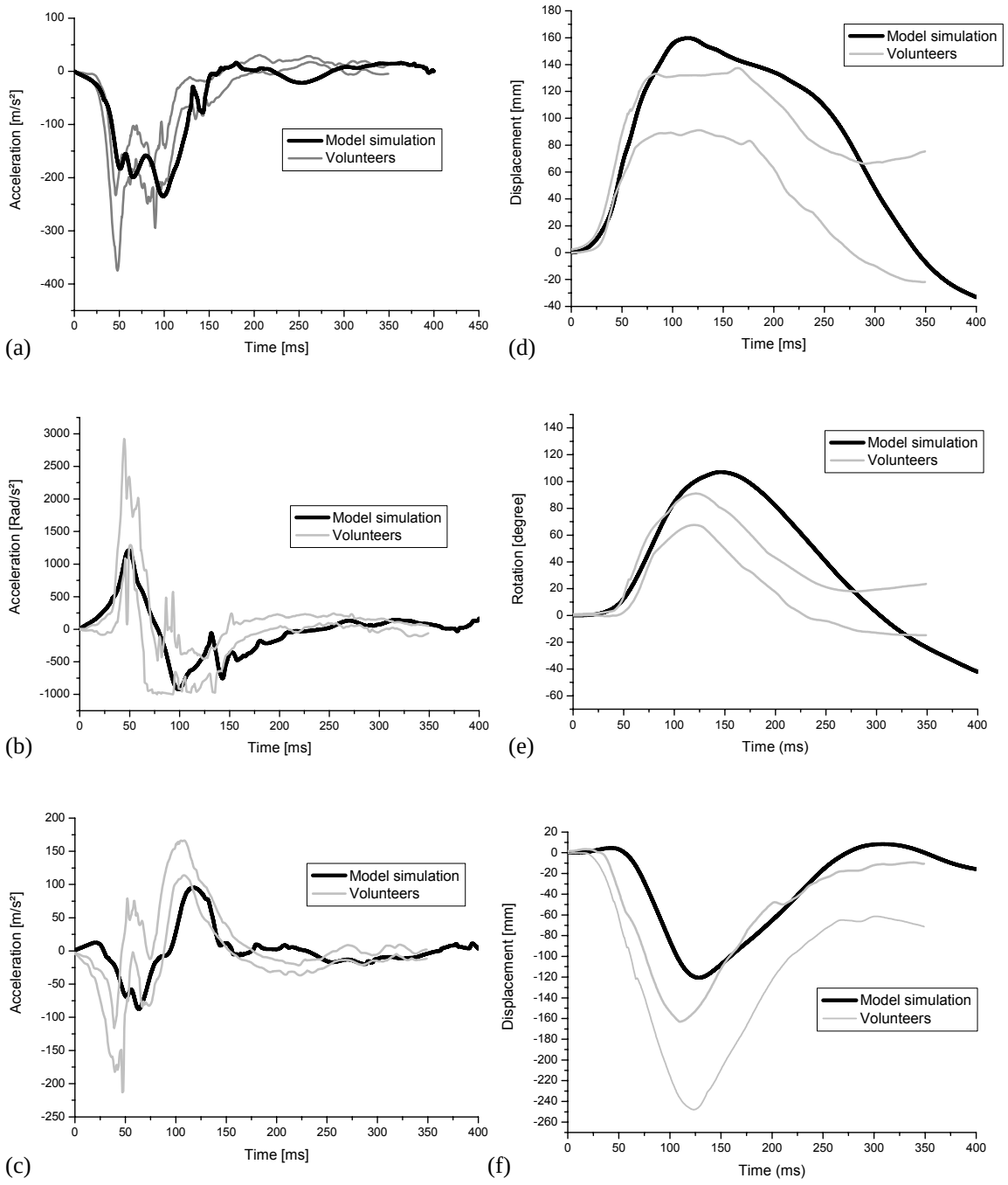

FIGURE 28. Temporal results of the neck FEM during the frontal impact after its frequency validation: (a) X-axis linear acceleration of the anatomical centre AC of the head, (b) Y-axis angular acceleration of the AC, (c) Z-axis linear acceleration of the AC, (d) X-axis displacement of the AC, (e) Rotation of the AC and (f) Z-axis displacement of the AC.

Temporal results of the neck FEM during the rear impact after its frequency validation.

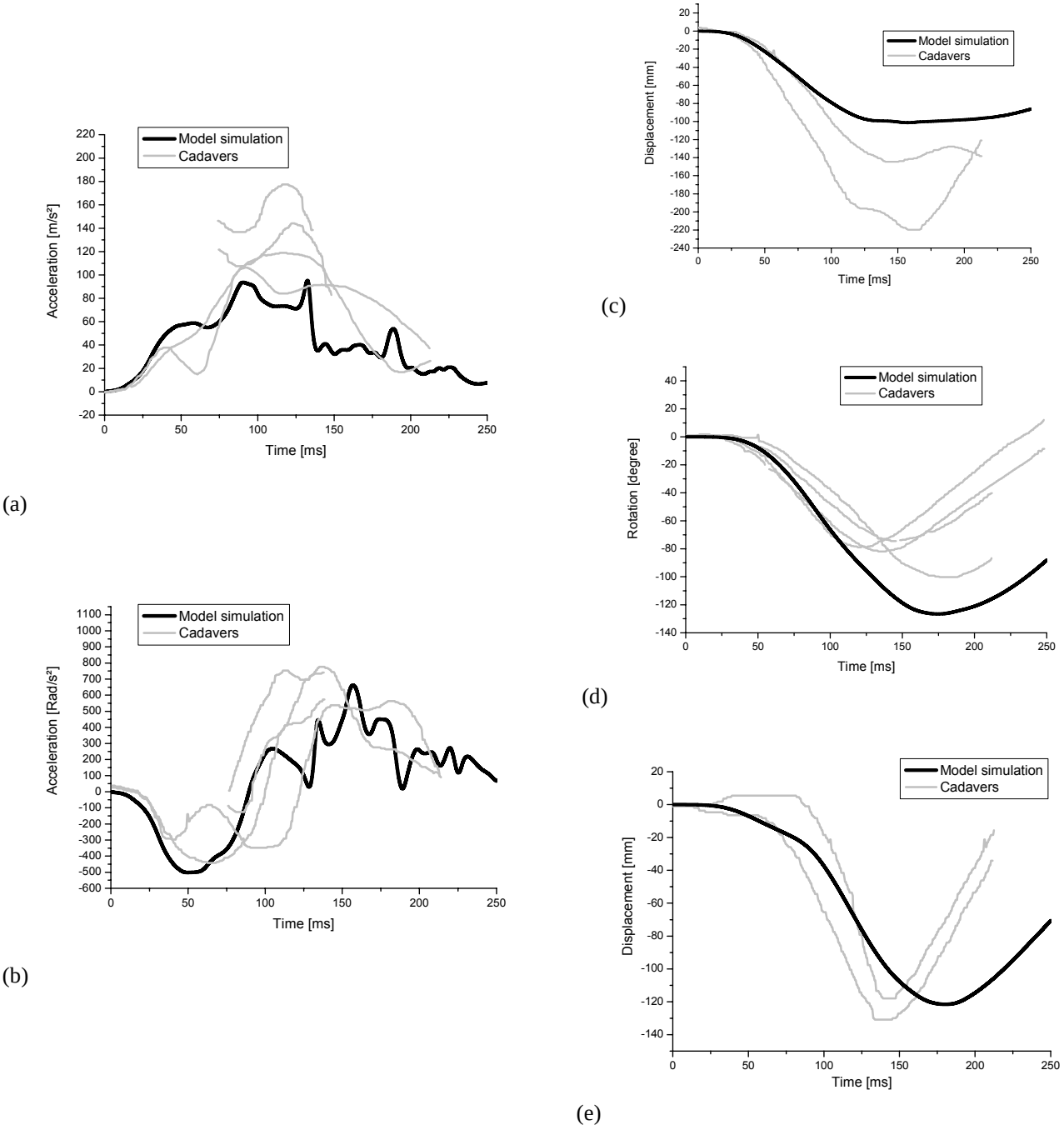

FIGURE 29. Temporal results of the neck FEM during the rear impact after its frequency validation : (a) Resultant acceleration of the AC, (b) angular acceleration of the AC., (c) X-axis displacement of the AC, (d) Rotation of the AC and (e) Z-axis displacement of the AC (Prasad et al. 1997).

Temporal results of the neck FEM during the oblique impact after its frequency validation.

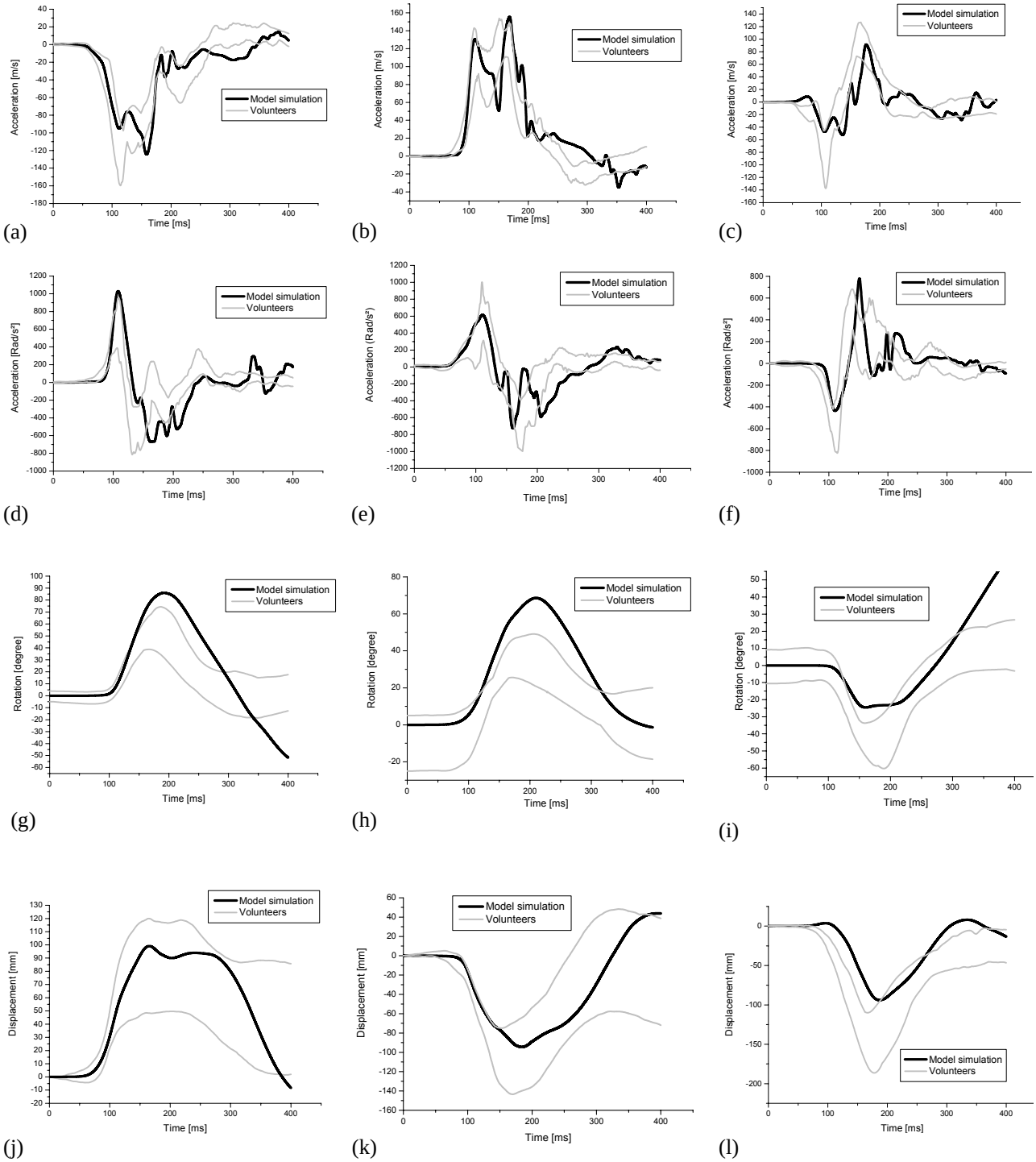

FIGURE 30. Temporal results of the neck FEM during the oblique impact after its frequency validation : X-axis (a), y-axis (b) and z-axis (c) linear accelerations of the AC respectively, x-axis (d), y-axis (e) and z-axis (f) angular accelerations of the AC respectively, x-axis (g), y-axis (h) and z-axis (i) rotation of the AC respectively and x-axis (j), y-axis (k) and z-axis (l) displacement of the AC respectively (N.B.D.L. Ewings et al. 1968, 1977).

Temporal results of the neck FEM during the lateral impact after its frequency validation.

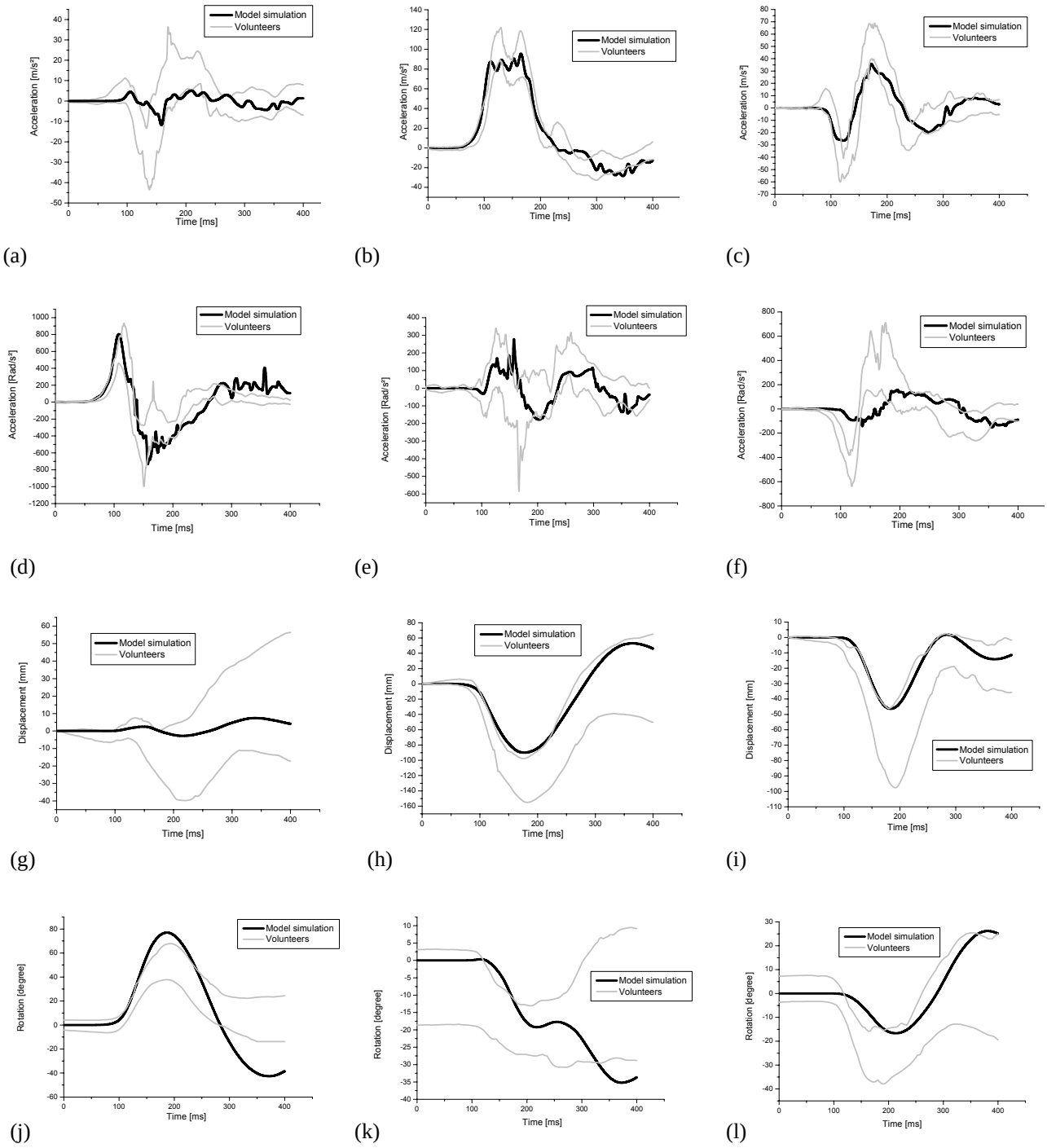

FIGURE 31. Temporal results of the neck FEM during the lateral impact after its frequency validation : X-axis (a), y-axis (b) and z-axis (c) linear accelerations of the AC respectively, X-axis (d), y-axis (e) and z-axis (f) angular accelerations of the AC respectively, X-axis (g), y-axis (h) and z-axis (i) rotation of the AC respectively and X-axis (j), y-axis (k) and z-axis (l) displacement of the AC respectively (N.B.D.L. Ewings et al. 1968, 1977).

DISCUSSION

The main discussion concerning the method is the hypothesis of linearity, doe to the assumption made at the transfer function definition level, but also in relation to the low impact energy involved in the experimental impact. It is therefore important to remember that the methodology is well designed to describe the neck behavior for low energy impact, or before non-linearity. Under these restrictions, how can modal analysis techniques, inform us about the complex properties of the human neck? Let us first recall that linear behavior has been checked in our experiments through the coherence function that remains between 0.9 and 1. Results illustrate the importance of mass distribution and damped elastic properties at the beginning of the motion. Resonance frequencies and mode shapes give the dynamic deformation initialization that may eventually continue until non-linearity appears in case of energetic impact.

The experimental vibration study under impulsive condition led to the identification of two natural frequencies at 1.3±0.1 Hz and 8±0.7 Hz associated with two separate deformation mode shapes. The new issue at this level is that the first mode at 1.3±0.1 Hz is associated with the neck extension and the second mode at 8±0.7 Hz a anterior-posterior retraction of the neck. It is important to mention here that five more human volunteer males have been submitted to the same test procedure and conduced to very similar results.

To the authors knowledge it is the first time that a head-neck FE model is validated against modal characteristics recorded in vivo. It was possible to fit both natural frequencies and the related mode shape by drastically modifying the ligament rigidity and dumping, two mechanical parameters reported in the literature with a very wide discrepancy.

With regard to the temporal validation of the FEM, we compared the response of our model with those of the literature. The figure B1 (Appendix B) superimposes the various responses of the models for the frontal impact. A statistical analysis was carried out for each authors (Appendix C, C1 table). The comparison of the statistical data in term of accelerations shows a better response of our model (initial and optimized) with 61.7% for the initial model, 53.9% for the optimized model, 34.3% for the Dauvilliers' model, 48.9% for the De Jager's model, 51% for the Astori's model and finally 36.85% for the Happee's model. Globally, the models of Astori and De Jager's model present better statistics, but it should be noted that for these two authors the displacement of the CG of the head are not available, but these kinematics' parameters are most difficult to validate.

Moreover, during the experimental test the initial condition at the first thoracic vertebrae was not clearly estimated. Ewing et al. (1969) reported that a rotation appears during the test that can explain the underestimated result for the z-axis displacement (9% for the initial model and 26% for the optimized model).

The figure B2 (Appendix B) shows the various curves of validations of several authors (Dauvilliers (1994), De Jager et al. (1996) and Astori et al. (1998)) for a lateral impact. No difference is observed between the initial model and the model optimized in frequency domain (73.3%). Moreover the response of our model is better than the authors' responses for this impact (Dauvilliers' model 39.3%, De Jager's model 58.6% and 62.8% for the model of Astori).

Concerning the oblique impact, the response of the optimized model is better than the initial model in terms of displacement, however we can note a reduction in the statistics for the angular accelerations. Globally, the response of the model remains acceptable with 66% of fidelity for the initial model and 62.1% for the model optimized in the frequency domain.

Finally, the results obtained in rear impact with the initial model and the optimized model do not present a great difference (53.4% and 51.9% respectively). However, we can note that the optimized model answers better in term of x-displacement (36.9% against 5.8%).

Thus, it appears that this model improvement or model optimization in the frequency domain has no significant influence on the temporal validation but permitted the adjustment of the anterior-posterior retraction mode. This illustrating the difficulty to validate correctly models under impact condition only in the temporal domain.

CONCLUSION

This study proposes the construction of a very close geometrical model of the cervical column of a given volunteer subject. With the mechanical parameters available from the literature it was possible to validate this model in the temporal domain as regards to the kinematics of the head in rear, front, lateral and oblique impact situations. The lack of precision in the mechanical properties of the models and the "width"

of the validation corridors led us to undertake a new characterisation of the cervical column in vivo based on modal analysis. This modal analysis based on the recording of the apparent mass in an impulse situation is restricted to the sagittal plane and reveals for the first time a flexion-extension mode at 1.3 Hz ± 0.1 and a retraction or translation mode at 8 Hz ± 0.7.

The option was then taken to carry out a numerical modal analysis of the model reproducing the experimental analysis. It appeared that for the initial model's mechanical parameters the flexion mode was appropriately reproduced, but the retraction motion was 16 times too rigid since its natural frequency was 4 times higher. An optimisation of the model in the frequency domain was obtained by reducing the damping and the rigidity of the upper ligaments. The two natural frequencies of the head-neck system were then faithfully reproduced by the model as well as the related mode shapes.

A classical temporal validation of the frequency domain optimised neck FE model was also performed and revealed no significant difference with the initial model. This result illustrates how difficult and how inefficient it is to validate complex systems against only temporal responses to impacts.

AKNOWLEDGMENT

The authors wish to thank I.R.C.A.D. (Institut de Recherche contre les Cancers de l'Appareil Digestif) for their contribution and the French ministry of research for their financial support (PREDIT n°00A008601).

REFERENCES

Astori, P. and Raballo, M. (1998) Multy-Body Numerical model of the Human Neck. Proc. Of the Int.Crashworthiness Conference pp 63-72.

Bendat, J. S. and Piersol, A. G. (1971) Random Data: Analysis and measurement procedure: Wiley-Interscience.

Camacho, D.L., Nightingale, R.W., Robinette, J.J., Vanguri, S.K., Coates, D.J. and Myers, B.S. (1997) Experimental Flexibility Measurements for the Development of a computational Head-Neck Model Validated for Near-Vertex Head Impact. Proc 41st Stapp Car Crash Conference, pp. 473-486. Society of Automotive Engineers, Warrendale, PA. Paper 973345.

Chazal, J., Tanguy, A., Bourges, M., Gaurel, G., Escande, G., Guillot, M. and Vanneuville, G. (1985) Biomechanical properties of spinal ligaments and a histological study of the supraspinal ligament in traction. Journal of Biomechanics (18)3 : 167-176.

Dauvilliers, F. (1994) Modélisation Tridimensionnelle et Dynamique du Rachis Cervical. PhD Thesis, ENSAM Paris.

De Jager, M., Sauren, A., Thunnissen, J. and Wismans, J. (1996) A Global and a Detailed Mathematical Model for Head-Neck Dynamics. Proc. 40th Stapp Car Crash Conference, pp. 269-281. Society of Automotive Engineers, Warrendale, PA. Paper 962430.

Deng, Y.-C. and Goldsmith, W. (1987) Response of a human head/neck/upper-torso replica to dynamic loading-II. Analytical/numerical model. Journal of Biomechanics 20(5) : 487-497.

Deng, B., Begeman, P.C., Yang, K.H., Tashman, S. and King, A.I. (2000) Kinematics of Human Cadaver Cervical Spine During Low Rear-End Impacts Proc. 44th Stapp Car Crash Conference, pp. 171-188. Society of Automotive Engineers, Warrendale, PA. Paper 2000-01-SC13.

Ejima, S., Wittek, A., Ono, K. and Yamasaki, K. (2003) Modification and validation of human neck model under direct head loading. Proc. 18th Enhanced Safety of Vehicles.

Ewing, C., Thomas, D., Patrick, L., Beeler, G. and Smith, M. (1968) Dynamic response of the head and neck of the living human to -Gx impact acceleration. Proc. 12th Stapp Car Crash Conference, pp. 424-439. Society of Automotive Engineers, Warrendale, PA. Paper 680792.

Ewing C., Thomas D., Beeler G., Patrick L. and Gillis D. (1969) Living human dynamic response to -Gx impact acceleration II - Accelerations measured on the head and neck. Proc. 13th Stapp Car Crash Conference, pp. 400-415. Society of Automotive Engineers, Warrendale, PA. . Paper 690817

Ewing, C., Thomas, D., Lustick, L., Muzzy, III W., Willems, G. and Majewski, P. (1977) Dynamic response of the human head and neck to +Gy impact acceleration. Proc. 21st Stapp Car Crash

Conference, pp. 549-586. Society of Automotive Engineers, Warrendale, PA. Paper 770928.

Halldin, P.H, Brolin, K., Kleiven, S. and Von Holst, H. (2000) Investigation of Conditions that Affect Neck Compression-Flexion Injuries Using Numerical Techniques. Proc 44st Stapp Car Crash Conference Society of Automotive Engineers, Warrendale, PA. Paper 2000-01-SC10.

Happee, R., Hoofman, M., Van den Kroonenberger, A.J., Morsink, P. and Wisman J. (1998) A Mathematical Human Body Model for Frontal and Rearward Seated Automotive Impact Loading. Proc. 42nd Stapp Car Crash Conference, pp. 75-88. Society of Automotive Engineers, Warrendale, PA. Paper 983150.

Kleinberger, M. (1993) Application of finite element techniques to the study of cervical spine mechanics. Proc. 37th Stapp Car Crash Conference, pp. 261-272. Society of Automotive Engineers, Warrendale, PA. Paper 933131.

Knudsen S. Torsiona elasticity of muscles (1953) Acta Physiologica Scandinavica.

Moroney S., Schultz A., Miller J. and Andersson G. (1988) Load-displacement properties of lower cervical spine motion segments. Journal of Biomechanics (21) 9: 769-779

Myers, B., McElhaney, J., Doherty, B., Paver, J. and Gray, L. (1991) The Role of Torsion in Cervical Spine Trauma. Spine 16(8) : 870-874.

Myers B., Van Ee C., Camacho D., Woolley T. and Best T. (1995) On the structural and material properties of mammalian skeletal muscle and its relevance to human cervical impact dynamics. Proc 39th Stapp Car Crash Conference, pp. 203-214. Society of Automotive Engineers, Warrendale, PA. Paper 952723,

Nitsche, S., Krabbel, G., Appel, H. and Haug, E. (1996) Validation of a Finite-Element-Model of the Human Neck. Proc. Ircobi Conference pp 107-122.

Ono, K., Kaneoka, K., Wittek, A. and Kajzer, J. (1997) Cervical Injury Mechanism Based on the Analysis of Human Cervical Vertebral Motion and Head-Neck-Torso Kinematics During Low Speed Rear Impacts. Proc. 41st Stapp Car Crash Conference, pp. 339-356. Society of Automotive Engineers, Warrendale, PA. Paper 973340.

Ovadia, D., Steinberger, E.L., Nissan, M. and Dekel, S. (2002) Whiplash injury-a retrospective study on patients seeking compensation. Injury 33(7) : 569-573.

Prasad, P., Kim, A. and Weerappuli, D.P.V. (1997) Biofidelity of Anthropomorphic Test Devices for Rear Impact. Proc. 41st Stapp Car Crash Conference, pp. 387-415. Society of Automotive Engineers, Warrendale, PA. Paper 973342.

Wen, N., Lavaste F., Santin J.J., Lassau J.P. (1993a) Three-dimensional biomechanical properties of the human cervical spine in vitro. I. Analysis of normal motion. Eur Spine J 2:2-11

Wen, N., Lavaste F., Santin J.J., Lassau J.P. (1993b) Three-dimensional biomechanical properties of the human cervical spine in vitro. II. Analysis of normal motion. Eur Spine J 2:12-15

Yang, K., Zhu, F., Luan, F., Zhao, L. and Begeman, P. (1998) Development of a Finite Element Model of the Human Neck. Proc. 42th Stapp Car Crash Conference, pp. 195-205. Society of Automotive Engineers, Warrendale, PA. Paper 983157.

Yoganadan, N., Kumarasan, S. and Pintar, S.A, (2001) Biomechaics of the cervical spine part 2. cervical spine soft tissues responses and biomechanical modelling. Clinical Biomechanics 16(1) : 1-27.

Yoganandan, N. and Pintar, F. (2001) A. Single rear impact produces lower cervical spine soft tissue injuries. Proc. Ircobi conference pp. 201-211.

APPENDIX A

TABLE A1. Material properties of the lower ligaments (Chazal et al. 1985, Yoganandan et al. 2001).

Ligament	Abbreviation	Level	Yoganadan (Exp)		Initial length (Exp)	Average of length (model)	Number of springs	Model (Chazal et al. 1985, Yoganandan et al. 2001)					
								α_1		α_2		α_3	
			Fc [N]	Dc [m]	Lo [mm]	Lo [mm]	-	F [N]	D [mm]	F [N]	D [mm]	F [N]	D [mm]
Anterior longitudinal ligament	ALL	C2-C3	92.76	5.79	18.8	5.37	7	0.42	0.34	3.29	1.29	3.78	1.65
		C3-C4				7.15	7	0.55	0.46	4.38	1.72	5.04	2.20
		C4-C5				5.95	8	0.40	0.38	3.19	1.43	3.67	1.83
		C5-C6	145.2	6.47	18.3	5.17	7	0.64	0.38	5.09	1.43	5.86	1.83
		C6-C7				5.69	10	0.49	0.42	3.92	1.57	4.15	2.01
		C7-T1				7.57	12	0.55	0.56	4.35	2.09	5.00	2.68
Posterior longitudinal ligament	PLL	C2-C3	71,07	3,45	19	4.91	5	0.44	0.22	3.26	0.69	3.67	0.89
		C3-C4				2.88	6	0.21	0.13	1.59	0.40	1.79	0.52
		C4-C5				3.46	6	0.26	0.16	1.92	0.48	2.16	0.63
		C5-C6	188,16	6,10	17.9	3.24	6	0.68	0.28	5.05	0.85	5.68	1.10
		C6-C7				3.11	7	0.56	0.26	4.16	0.82	4.67	1.06
		C7-T1				5.34	8	0.84	0.45	6.24	1.40	7.02	1.82
Flavum ligament	FL	C2-C3	121.44	6.54	8.5	5.18	12	1.29	1.12	5.42	3.03	6.17	3.98
		C3-C4				6.83	14	1.46	1.47	6.13	3.99	6.97	5.26
		C4-C5				6.72	12	1.68	1.45	7.04	3.93	8.00	5.17
		C5-C6	9,370	129,09	10.6	4.88	12	1.04	1.21	4.36	3.28	4.95	4.31
		C6-C7				4.71	13	0.92	1.17	3.88	3.17	4.41	4.16
		C7-T1				7.38	10	1.89	1.83	7.90	4.96	8.98	6.52
Capsular ligament	CL	C2-C3	10,24	119,63	6.92	2.44	24	0.26	0.94	1.55	2.74	1.75	3.61
		C3-C4				3.39	28	0.31	1.30	1.84	3.81	2.09	5.01
		C4-C5				3.38	30	0.29	1.3	1.71	3.80	1.95	5.00
		C5-C6	7,79	181,05	6.72	3.72	28	0.53	1.12	3.15	3.28	3.58	4.31
		C6-C7				2.64	31	0.34	0.79	2.02	2.33	2.29	3.06
		C7-T1				3.84	34	0.45	1.16	2.68	3.38	3.04	4.45
Interspinous ligament	ISL	C2-C3	6,33	38,61	10.4	11.29	5	1.42	2.06	7.29	5.17	8.38	6.87
		C3-C4				9.94	5	1.25	1.81	6.42	4.54	7.38	6.05
		C4-C5				7.91	5	0.99	1.44	5.11	3.61	5.87	4.81
		C5-C6	6,74	38,59	9.9	14.04	4	2.32	2.86	11.9	7.17	13.68	9.56
		C6-C7				8.74	6	0.96	1.78	4.94	4.46	5.67	5.95
		C7-T1				14.70	6	1.62	3.00	8.30	7.50	9.55	10.01

APPENDIX A Continued.

TABLE A2. Material properties of the upper ligaments (Chazal et al. 1985, Yoganandan et al. 2001).

Ligament	Level	Yoganadan (Exp)		Value implement	Average of length (model)	Number of springs	Model (Chazal et al. 1985, Yoganandan et al. 2001)					
							α_1		α_2		α_3	
		Fc [N]	Dc [mm]	Fc [N]	Lo [mm]		D [mm]	F [N]	D [mm]	F [N]	D [mm]	Fc [N]
Capsular ligament	**C2-C1**	314	9.3		3,83	28	2,34	0,86	6,84	5,03	9,00	5,71
Ligament posterior	**C2-C0**			83	40,38	3	5,20	4,15	15,20	24,35	20,00	27,67
Atloidien-axoidien anterior	**C2-C1**	263	11.8		11,93	6	3,07	6,58	8,97	38,57	11,80	43,83
Transversal ligament	**C2-C1**			200	5,40	6	1,30	5,00	3,80	29,33	5,00	33,33
Ligament flavum	**C2-C1**	111	9.6		13,62	14	2,50	1,19	7,30	6,98	9,60	7,93
Ligament posterior	**C2-C1**			71	22,62	3	1,30	3,55	3,80	20,83	5,00	23,67
Transversal axoidien	**C2-C1**			436	9,78	7	3,25	9,34	9,50	54,81	12,50	62,29
Occipital transversal	**C2-C0**			250	8,34	4	1,30	9,38	3,80	55,00	5,00	62,50
Ligament posterior	**C1-C0**	83	18.1		16,74	4	4,71	3,11	13,76	18,26	18,10	20,75
Occipito-atloidien anterior	**C2-C0**			232	44,14	6	4,91	5,80	14,36	34,03	18,90	38,67
Ligament flavum	**C0-C1**			83	15,23	5	4,71	2,49	13,76	14,61	18,10	16,60
Alar ligament	**C0-C2**	357	14.1		7,28	6	3,67	8,93	10,72	52,36	14,10	59,50
Membrane tectoria	**C0-C2**	76	11.9		27,48	3	3,09	3,80	9,04	22,29	11,90	25,33
Capsular ligament	**C1-C0**	320	9.9		5,26	26	2,42	0,92	7,07	5,42	9,30	6,15
Apical ligament	**C2-C0**	214	8		3,36	2	2,08	16,05	6,08	94,16	8,00	107,00
Occipito-atloidien lateral	**C1-C0**			100	8,66	6	5,20	2,50	15,20	14,67	20,00	16,67

APPENDIX B

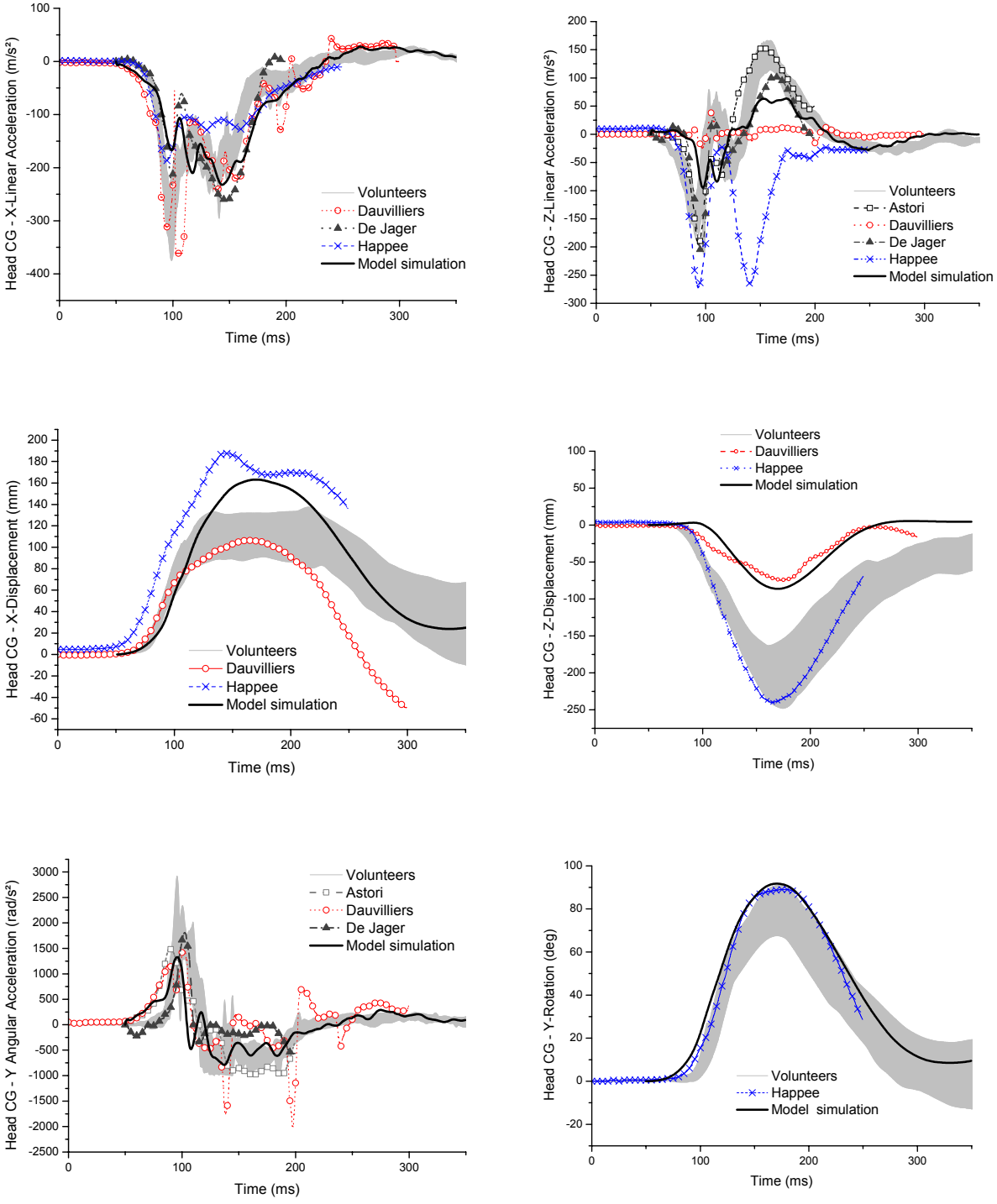

FIGURE B1. Different models' responses during the frontal impact (Dauvilliers (1994), Astori et al. (1998), DeJager et al. (1996), Happee et al. (1998), and the initial model).

APPENDIX B Continued.

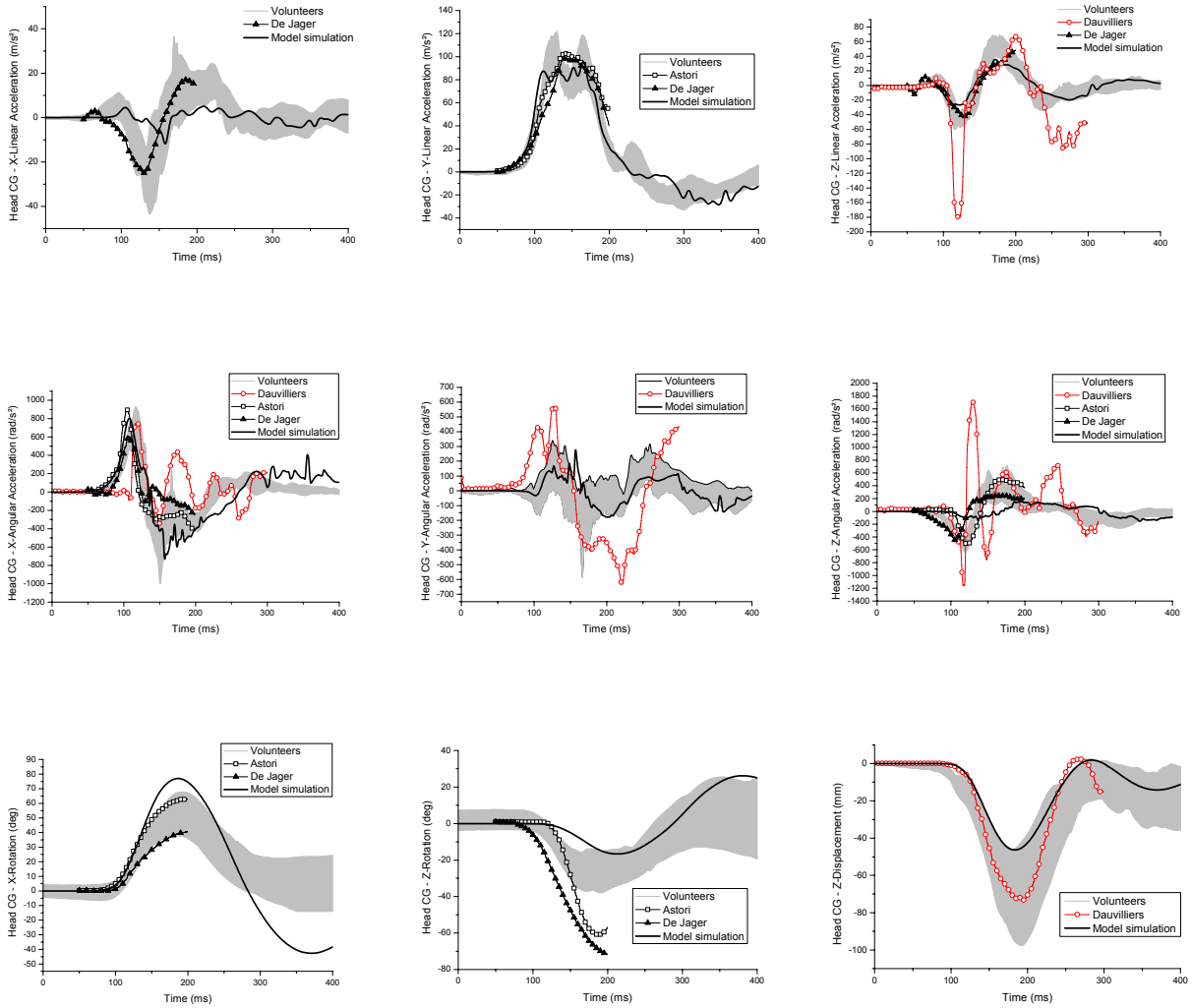

FIGURE B2. Different models' responses during the lateral impact (Dauvilliers (1994), Astori et al. (1998), DeJager et al. (1996), and the initial model).

APPENDIX C.

TABLE C1. Summary table of the various statistics obtained for the frontal impact.

	Acx	Ary	Acz	Dx	Ry	Dz	Mean
Initial model	57.4%	74.3%	53.4%	67.9%	49.8%	9%	**51.9%**
Optimised model	42.4%	66.3%	53.1%	47%	38.8%	26%	**45.6%**
Dauvilliers	36.5%	28.9%	37.5%	64.1%	-	19.6%	**37.3%**
De Jager	44.5%	50.7%	51.6%	-	-	-	**48.9%**
Astori	-	44.7%	57.3%	-	-	-	**51%**
Happee	43.9%	-	29.8%	0%	69.5%	60.8%	**40.8%**

TABLE C2. Summary table of the various statistics obtained for the lateral impact.

	Acx	Acy	Acz	Arx	Ary	Arz	Dx	Dy	Dz	Rx	Ry	Rz	Mean
Initial model	83.9%	75.4%	85.9%	51.2%	87.7%	58.9%	93.9%	69.4%	79.8%	50.5%	71.3%	72.3%	**73.3%**
Optimised model	83.9%	75.4%	85.7%	51.2%	87.5%	58.9%	93.9%	69.5%	79.8%	50.5%	71.3%	72.2%	**73.3%**
Dauvilliers	-	-	37%	51.9%	36.5%	38.4%	23.9%	41.8%	73%	-	11.7%	-	**39.3%**
De Jager	69.6%	61.4%	64%	54.7%	-	54.2%	-	-	-	76%	-	30%	**58.6%**
Astori	-	65.9%	-	65.7%	-	37.7%	-	-	-	82.7%	-	61.9%	**62.8%**

TABLE C3. Summary table of the various statistics obtained for the oblique impact.

	Acx	Acy	Acz	Arx	Ary	Arz	Dx	Dy	Dz	Rx	Ry	Rz	Mean
Initial model	73.4%	75.1%	67.8%	65.6%	72.9%	80.3%	91.9%	69%	27.3%	75.7%	46.3%	47.4%	**66.1%**
Optimised model	70.7%	57.9%	60.6%	51.3%	50.8%	58.8%	95.4%	95%	42.8%	53%	50.8%	58%	**62.1%**

TABLE C4. Summary table of the various statistics obtained for the rear impact.

	Resultant acceleration	Ary	Dx	Dz	Ry	Mean
Initial model	31%	60.3%	5.8%	70.2%	100%	**53.5%**
Optimised model	40.3%	67%	36.9%	65.4%	50%	**51.9%**

With Acα : α-Axis linear acceleration, Arα : α-Axis angular acceleration, Dα : α-Axis displacement, Rα : α-Axis rotation.